Volume 51
Number 18
21 September 2022
Pages 7685–8142

Chem Soc Rev

Chemical Society Reviews

rsc.li/chem-soc-rev

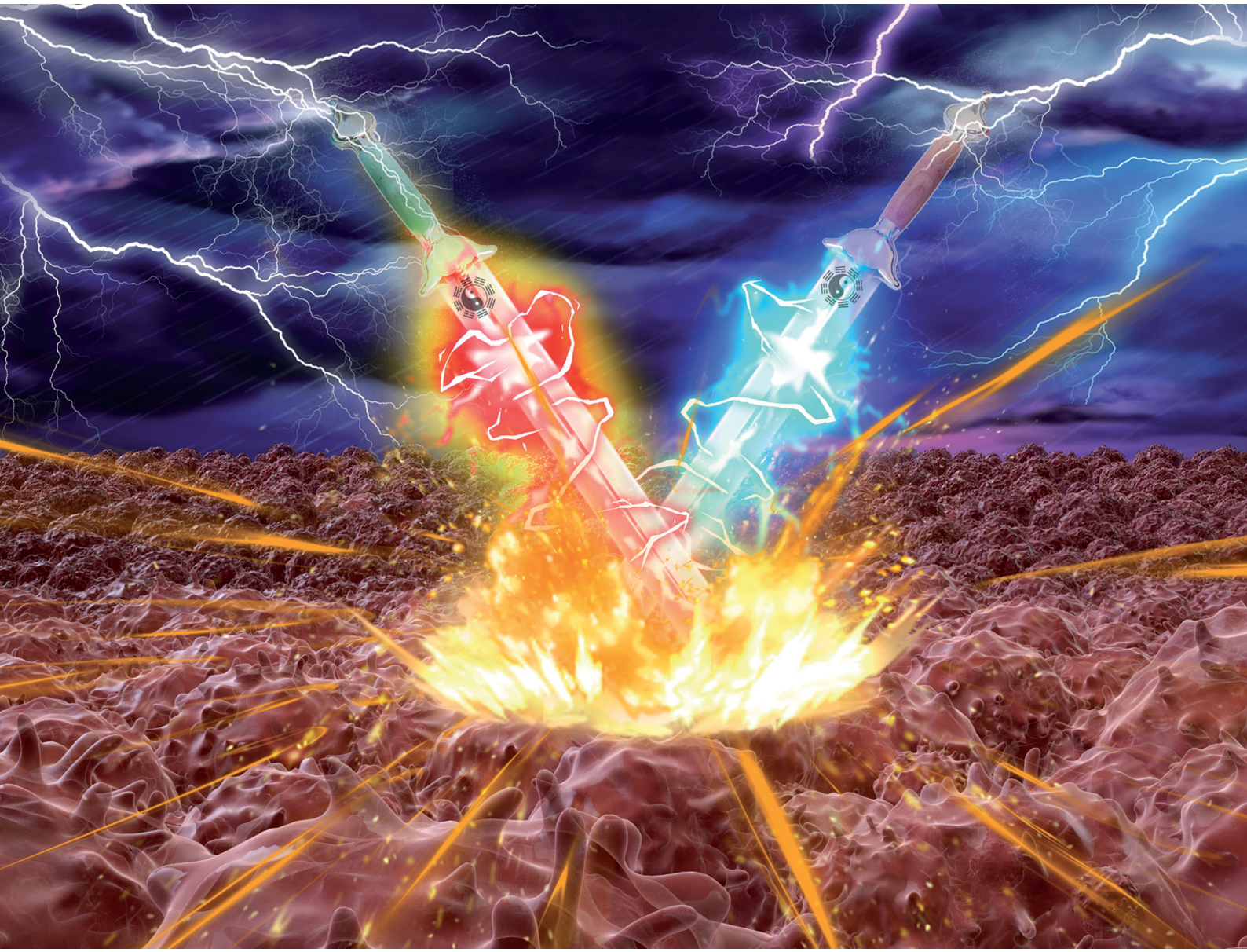

ISSN 0306-0012

ROYAL SOCIETY OF CHEMISTRY

TUTORIAL REVIEW

Peng Huang, Xiaoyuan Chen *et al.*

Management of fluorescent organic/inorganic nanohybrids for biomedical applications in the NIR-II region

Chem Soc Rev

TUTORIAL REVIEW

View Article Online
View Journal | View Issue

Cite this: *Chem. Soc. Rev.*, 2022, **51**, 7692

Management of fluorescent organic/inorganic nanohybrids for biomedical applications in the NIR-II region

Benhao Li,†[abcd] Mengyao Zhao,†[bcd] Jing Lin,[a] Peng Huang*[a] and Xiaoyuan Chen*[bcd]

Received 19th May 2022

DOI: 10.1039/d2cs00131d

rsc.li/chem-soc-rev

Biomedical fluorescence imaging in the second near-infrared (NIR-II, 100–1700 nm) window provides great potential for visualizing physiological and pathological processes, owing to the reduced tissue absorption, scattering, and autofluorescence. Various types of NIR-II probes have been reported in the past decade. Among them, NIR-II organic/inorganic nanohybrids have attracted widespread attention due to their unique properties by integrating the advantages of both organic and inorganic species. Versatile organic/inorganic nanohybrids provide the possibility of realizing a combination of functions, controllable size, and multiple optical features. This tutorial review summarizes the reported organic and inorganic species in nanohybrids, and their biomedical applications in NIR-II fluorescence and lifetime imaging. Finally, the challenges and outlook of organic/inorganic nanohybrids in biomedical applications are discussed.

Key learning points

(1) Advantages of organic/inorganic nanohybrids for biomedical applications in the NIR-II region.
(2) Typical organic and inorganic species as building blocks for the construction of NIR-II nanohybrids.
(3) Design strategies of NIR-II nanohybrids for fluorescence and luminescence intensity-based and lifetime-based bioimaging and biosensing.
(4) Notable examples from the literature to highlight the various design strategies and biomedical applications.
(5) Perspectives of the future development of NIR-II organic/inorganic nanohybrids.

1. Introduction

Optical biomedical imaging is a powerful imaging technique in life science for real-time monitoring of physiological and pathological processes due to its non-invasiveness, non-ionizing radiation, high sensitivity, and high spatiotemporal resolution.[1–3] Recently, newly emerged fluorescence imaging in the second near-infrared (NIR-II, 1000–1700 nm) window, which is also called the shortwave infrared (SWIR) window, has attracted widespread attention in the biomedical field.[4–6] Photons in the NIR-II range provide a better opportunity for biological imaging owing to the high resolution at deeper tissue penetration (~5–20 mm) as compared to light in visible (400–700 nm) and NIR-I (700–900 nm) regions because of the decreased tissue absorption, scattering, and autofluorescence.[7–9] Along with the development of fluorescence imaging, a more careful definition of the NIR region has emerged, including NIR-II (900–1300 nm), NIR-IIa (1300–1400 nm), NIR-IIx (1400–1500 nm), NIR-IIb (1500–1700 nm), NIR-IIc (1700–1800 nm), and NIR-III (2080–2340 nm).[10] According to a previously reported theoretical model, $\delta = \left[3\mu_a\left(\mu_a + \mu_s'\right)\right]^{-1/2}$, where δ is the theoretical penetration depth of the photon in bio-tissue, μ_a is the absorption extinction coefficient, and μ_s' is the reduced scattering coefficient, which is directly proportional to λ^{-w} (λ is the excitation or emission wavelength, and the

[a] *Marshall Laboratory of Biomedical Engineering, International Cancer Center, Laboratory of Evolutionary Theranostics (LET), School of Biomedical Engineering, Shenzhen University Health Science Center, Shenzhen 518060, China. E-mail: peng.huang@szu.edu.cn*
[b] *Departments of Diagnostic Radiology, Surgery, Chemical and Biomolecular Engineering, and Biomedical Engineering, Yong Loo Lin School of Medicine and Faculty of Engineering, National University of Singapore, Singapore, 119074, Singapore. E-mail: chen.shawn@nus.edu.sg*
[c] *Clinical Imaging Research Centre, Centre for Translational Medicine, Yong Loo Lin School of Medicine, National University of Singapore, Singapore 117599, Singapore*
[d] *Nanomedicine Translational Research Program, NUS Center for Nanomedicine, Yong Loo Lin School of Medicine, National University of Singapore, Singapore 117597, Singapore*
† B. Li, and M. Zhao contributed equally to this work.

exponent w ranges from 0.22 to 1.68 depending on the different scatterers in biological tissues).[11,12] Thus, it is obvious that the tissue penetration depth of photons will be enhanced with the bathochromic shift of both excitation and emission wavelengths.[13] For example, NIR-II imaging of mouse lymph vessels exhibited a higher signal-to-background ratio (SBR) beyond 1100 nm (SBR = 3.3) compared to those in the visible (SBR = 1.4 at 520 nm) and NIR-I (SBR = 1.3 at 720 nm) regions. Moreover, the bathochromic shifted signal collection window beyond 1300 nm and 1500 nm further provided optimized imaging contrast (SBR = 7.3 and 10.5, respectively).[14] Besides the imaging collection window, excitation with a longer wavelength also exhibits superior spatial resolution and deeper tissue penetration. The NIR-II hindlimb blood vessel images under NIR-II 1064 nm excitation (SBR = 4.32) have been demonstrated with much higher SBR than those under shorter wavelength (655–980 nm) excitation (SBR = 1.9–2.2).[13] Thus, NIR-II bioimaging is a desired technique for high spatially resolved bio-detection under deep penetration depth and real-time physiological monitoring *in vivo*.

Fluorescence (or luminescence) lifetime as an intrinsic property of fluorescent (or luminescent) materials has also been investigated for *in vitro* and *in vivo* imaging and sensing. It refers to the average time that the photon stays in its excited state before transiting back to the ground state.[15] Compared with traditional intensity-based imaging, lifetime-based imaging can report on physiological and pathological events more reliably owing to the independence of material concentration, excitation laser power, and unknown tissue penetration depth.[16] It has been widely used for intracellular ion detection, and tumor hypoxia quantification.[17,18] The premise of fluorescence (or luminescence) lifetime imaging is that the photons emitted from materials are received by the imaging detectors. Thus, the optical materials with longer emission and excitation wavelengths are more suitable for fluorescence (or luminescence) lifetime imaging in deep biological tissues.

So far, a lot of optical materials, including rare-earth doped nanoparticles (RENPs),[19] quantum dots (QDs),[20] organic dyes,[21,22] metal–ligand complexes,[23] single-walled carbon nanotubes,[24] and semiconducting polymer nanomaterials[5]

Benhao Li

Benhao Li received his PhD. degree from Fudan University in 2020. Now he is working as a research fellow at the National University of Singapore (NUS) under supervision of Prof. Xiaoyuan (Shawn) Chen. His current research focuses on NIR bioimaging and biosensing, and gene therapy.

Mengyao Zhao

Mengyao Zhao received her BS degree from Nankai University in 2015 and PhD degree from Fudan University in 2020. Her current research interests focus on lanthanide-based materials for biomedical imaging, sensing, and therapy.

Jing Lin

Jing Lin is a Distinguished Professor at the School of Biomedical Engineering, Shenzhen University Health Science Center, China. She received her PhD in Organic Chemistry from the Donghua University and Shanghai Institute of Organic Chemistry, Chinese Academy of Sciences in 2010. After two years, she moved to the United States of America and spent 4 years as a postdoc at the University of Maryland and the National Institutes of Health (NIH). She joined the faculty of Shenzhen University (SZU) in 2016 and was promoted as a Distinguished Professor in 2018. Her research focuses on molecular imaging, nanomedicine and theranostics.

Peng Huang

Peng Huang is a Distinguished Professor, Chief of the Laboratory of Evolutionary Theranostics (LET), and Director of the Department of Molecular Imaging, at the School of Biomedical Engineering, Shenzhen University Health Science Center, China. He received his PhD degree in Biomedical Engineering from the Shanghai Jiao Tong University in 2012. He then joined the Laboratory of Molecular Imaging and Nanomedicine (LOMIN) at the National Institutes of Health (NIH) as a postdoctoral fellow. In 2015, he moved to Shenzhen University as a Distinguished Professor. His research focuses on molecular imaging, nanomedicine and theranostics.

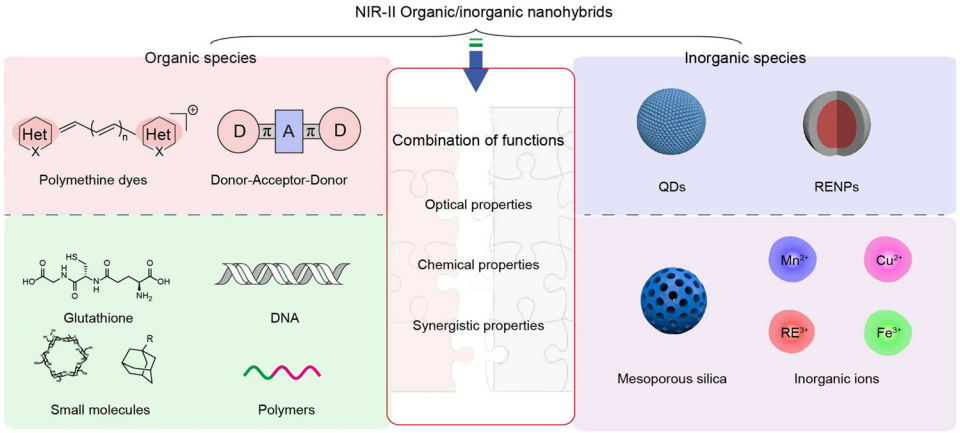

Fig. 1 Exemplary organic species and inorganic species as building blocks to construct NIR-II nanohybrids. Organic species are mainly divided into polymethine and donor–acceptor–donor (D–A–D) dyes with NIR optical properties, and functional small molecules (such as glutathione, DNA) and polymers without NIR optical properties. Inorganic species consist of quantum dots (QDs) and rare-earth doped nanoparticles (RENPs) with NIR-II emission, and functional mesoporous silica, inorganic ions.

have been developed for NIR-II fluorescence (or luminescence) intensity-based or lifetime-based bio-imaging and bio-detection, such as cancer imaging, biomolecules, and biomarker detection. These materials could be generally divided into organic and inorganic materials (Fig. 1). NIR-II organic materials show many advantages, including good biocompatibility, diverse chemical structures, and facile molecular modification. However, there are also some limitations such as poor photostability and weak chemical stability. In contrast, NIR-II inorganic materials hold good stability and robust spectral properties, which are suitable for long-time imaging, while the superior stable optical properties, on the other hand, hinder their usage as sensors. Thus, in response to the growing requirement of imaging and sensing sensitivity and reliability, NIR-II organic/inorganic nanohybrids are developed with advantages of both organic and inorganic species.[25] Surprisingly, besides integrating the advantages, the hybrids also exhibit new properties through the synergy of organic and inorganic components, such as organic induced crosslinking of inorganic nanoparticles, inorganic led organic molecule aggregation, and energy transfer between the organic and inorganic species. By rational design of the composition, combination strategy, size, and morphology, versatile functions and optical properties can be realized. Therefore, NIR-II organic/inorganic nanohybrids have great potential in the biomedical field.

This tutorial review aims to summarize the recent progress in various types of organic/inorganic nanohybrids for biomedical applications in the NIR-II region, such as tumor imaging, inflammation visualization, biomolecule detection, and so on. In particular, we summarize the design strategies of NIR-II organic/inorganic nanohybrids, including (i) organic–organic component interaction induced nanohybrid aggregation and disaggregation; (ii) inorganic components as carriers mediating J-aggregates formation; (iii) fluorescence (or luminescence) intensity and lifetime biosensors based on energy transfer, dye sensitizing methods, secondary absorption, absorption competition-induced emission (ACIE), or dual emitting systems between organic and inorganic species.

Xiaoyuan Chen

Prof. Xiaoyuan (Shawn) Chen received his PhD in Chemistry from the University of Idaho (1999). After being a faculty at the University of Southern California and Stanford University and then Senior Investigator/Lab Chief at the National Institutes of Health, he is now Nasrat Muzayyin Professor in Medicine and Technology, Yong Loo Lin School of Medicine and Faculty of Engineering, National University of Singapore. His current research interests are mainly theranostics (radiotheranostics, nanotheranostics, immunotheranostics, magnetotheranostics, phototheranostics, etc.) that can be clinically translatable. He has published over 900 papers and numerous books (H index, 170).

2. Construction of NIR-II organic/inorganic nanohybrids

2.1 Organic species

Organic species as building blocks for the construction of NIR-II nanohybrids can be divided into two categories. The first kind is small organic molecules with optical characteristics (absorption and emission), including polymethine dyes, donor–acceptor–donor (D–A–D) dyes, boron dipyrromethene (BODIPY) dyes, and others.[26,27] The second kind is small molecules without NIR-II optical properties but exhibit responsive or recognition functions, such as polymers, DNA, glutathione (GSH), cyclodextrin (CD)–adamantane analogs of host–guest pairs, and so on.[25]

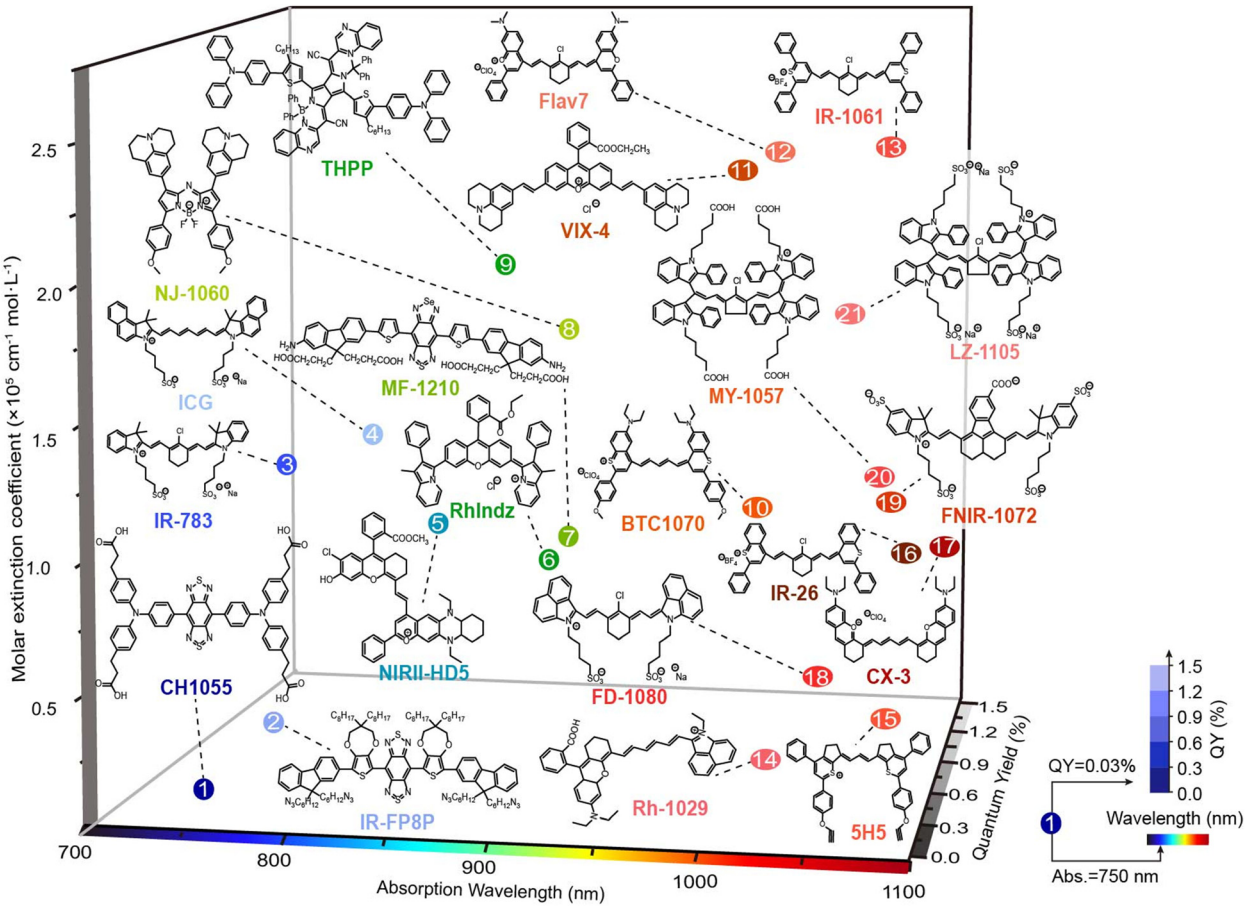

Fig. 2 3D plot of molar extinction coefficient and quantum yield *versus* the maximum absorption wavelength for the major classes of organic dyes for NIR-II bio-application. The color and transparency of number indicate its maximum absorption wavelength and quantum yield, respectively.

2.1.1 Organic dyes with optical properties. With the rapid development of NIR-II bioimaging and biosensing, a plethora of molecular dyes has been designed. Polymethine, D–A–D, and BODIPY dyes are three main types of organic structures with optical properties. The typical molecules with their optical properties are summarized in Fig. 2. Besides some molecules with excitation and emission wavelengths within 1000 nm which have been treated as NIR-II contrast agents using the emission tail fluorescence into the NIR-II window (such as indocyanine green (ICG), IR-783, IR-12N3, and IRDye800CW[28–30]), more molecules with maximum emission, even maximum excitation beyond 1000 nm, were developed. From the clinically used NIR-I ICG, to the NIR-II emitting small molecular contrast agent CH1055, then to NIR-II exciting FD-1080, small molecular dyes showed their superior *in vivo* imaging resolution and contrast. In addition to these advantages, the combination with inorganic materials will further burst new diversities and more possibilities.

In organic/inorganic nanohybrids, molecular dye as an organic component plays an important role in Förster resonance energy transfer (FRET), dye sensitizing methods, secondary absorption, ACIE, and dual emitting systems, which will be discussed in detail in Section 4. In general, organic molecular dyes may realize their function as two roles: emitters, or absorbers, which correspondingly require different properties. Hence, the optical properties of the reported organic dyes (whether or not to be used to construct organic/inorganic nanohybrids) will be introduced from two aspects: (i) molecular dyes with high brightness are suitable as emitters. Among them, most of the D–A–D dyes and BODIPY dyes with superior photo- and chemical-stability and robust emission intensity can be used as constant calibrated reference emitters in ratiometric fluorescence imaging, such as D–A–D structural CH1055,[31] Q4,[32] CH4-T,[33] IR-FE,[34] IR-FP8P,[35] H1,[21] IR-FTAP,[36] H2a-4T,[37] HLZ-BTED,[38] 68Ga-SCH2,[39] pFE[40] and MF-1210,[41] and BODIPY dyes NAB,[42] NJ-1060,[43] WH-4,[44] ZX-NIR,[45] ABDPTPA,[46] RhIndz[47] and THPP.[48] In contrast, some other molecular dyes exhibit structural and spectral responsiveness towards the disease microenvironment. For instance, polymethine dyes, especially heptamethine cyanine dyes, are responsive to reactive species, including oxygen/nitrogen reactive species, ROS and RNS, leading to the structure destruction and fluorescence intensity decrease. Typical heptamethine cyanine dyes are ICG,[28] MY-1057,[49] and A1094.[50] Besides, some polymethine dyes and BODIPY dyes could be further modified to realize specific responsiveness. For example, the reported LET-1052,[51] APNO-1080,[52] and ZX-NIR[45] showed a "turn-on" fluorescence or absorption signal in the presence of H^+, NO, and H_2S, respectively. These molecular dyes thus could be used to construct activatable nanosensors to light up the

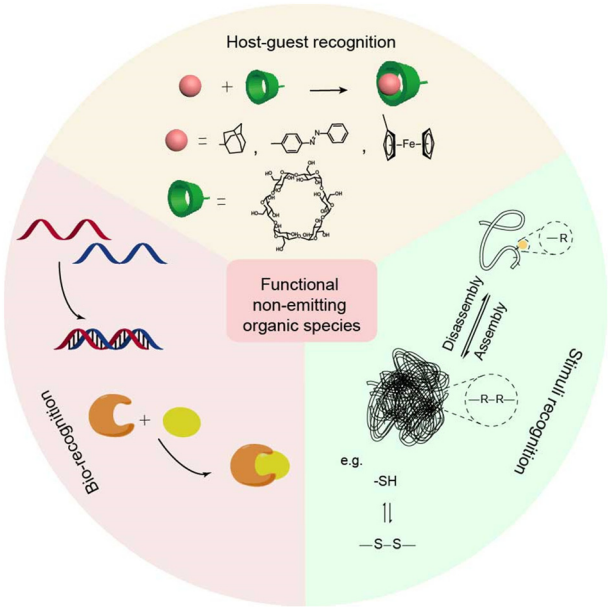

Fig. 3 The functional organic species without NIR optical properties and their interactions, including host–guest recognition, bio-recognition, and stimulus recognition in NIR-II organic/inorganic nanohybrids. For host–guest recognition, the pink spheres represent guest molecules, such as adamantane, azobenzene, ferrocene, *etc.* The green columns represent host molecules, such as cyclodextrin, crown ether, *etc.* Bio-recognition includes complementary base pairing of DNA and biotin–avidin recognition. For stimulus recognition, assembly/disassembly of materials can be achieved under formation and cleavage of covalent bonds.

disease lesions. (ii) Molecular dyes with high absorption cross-section and extinction coefficient could serve as absorbers. In FRET and secondary absorption systems, molecular dyes absorb and quench the emission light of inorganic emitters to quench the fluorescence signal or influence luminescence lifetime (MY-1057,[49] Flav7,[53] 5H5,[54] CX-3,[55] BTC1070,[56] Rh-1029,[57] VIX-4,[58] NIRII-HD5,[59] LET-1052,[51] NRh,[42] NIR-1380,[60] and FNIR-1072.[61]). However, in dye sensitizing and ACIE systems, molecular dyes absorb excitation light, and then either transfer energy to emitters (in a dye sensitizing system, such as ICG,[62] ALK-pi,[63] and NPh[64]) or quench the emitters (in ACIE systems, such as IR-808,[65] and NPTAT[66]). In these circumstances, organic molecular dyes are usually required to endow nanohybrids with "on–off" signals. As a matter of fact, many organic molecular dyes hold both high brightness and strong absorbing ability, making them suitable to be an emitter or absorber in different nanohybrids. Thus, researchers may take full advantage of these molecules and their properties instead of constraining them within a fixed role during hybrid designing.

2.1.2 Functional organic components without optical properties. Functional organic components without NIR absorption or emission properties are another class of organic species as building blocks for the construction of NIR-II organic/inorganic nanohybrids (Fig. 3). Combining the rationally designed functional organic species with an inorganic component will endow nanohybrids with tunable properties and lay the foundation for versatile biomedical applications. In most cases, functional organic components drive the inorganic nanoparticles to assemble and disassemble, producing varying optical emission signals for bioimaging and biosensing.[67] Their responsiveness and function mainly include host–guest recognition, bio-recognition, and stimulus recognition.[19,68]

Host–guest molecular recognition provides an opportunity for the construction of assembly and disassembly, allowing the size of the assembly to be regulated at the molecular level. Thus, it opens a path for the construction of intelligent systems.[19] Typical macrocyclic compounds, such as cucurbituril (CB), cyclodextrin (CD), and calixarene, can act as hosts with a hydrophilic outer shell and a hydrophobic cavity, and bind with guests *via* noncovalent interactions. Macrocyclic compounds can be modified onto the surface of inorganic species, thus acting as "host–guest recognition groups" to further functionalize organic–inorganic nanohybrids.[69] Therefore, host–guest molecules on the surface of inorganic species can initiate the assembly of nanohybrids to form large aggregates, thereby prolonging the retention time of nanohybrids at lesions and improving the SBR during bioimaging. For instance, small sized AuNPs modified with quaternary ammonium were easily taken up and pumped out by MCF-7 cells. While after adding CB, aggregates were formed through interaction between benzyl units and CB, thereby allowing prolonged intracellular retention time of nanohybrids.[70]

Bio-recognition, such as DNA base pairing and biotin–avidin recognition between nanohybrids would also cause assembly. Biomolecules with bio-recognition ability are suitable for surface modification of their inorganic components for bioimaging and biosensing due to high biocompatibility. DNA as a typical bio-recognition molecule has been used for crosslinking of inorganic nanoparticles.[71] In general, 20–40 base pairs of complementary single-stranded DNA fragments are immobilized on the surface of different nanoparticles, respectively. The assembly between nanohybrids is easy to achieve when the target DNA binds to the complementary sequence of the captured DNA. For example, the surfaces of AuNPs were decorated with a sequence of i-motifs. The aggregates of AuNPs would be formed along with the construction of the i-motif structure under acidic conditions, thereby enhancing the accumulation of nanohybrid at lesions.

Besides the above-mentioned specific recognition, many small molecules exhibit various physical properties and reactivities. Stimulus recognition is one of the principles for the design of smart nanohybrids. Active nanohybrids mainly depend on the design of organic species. The flexible organic species, such as cyanine dyes, allow intelligent chemical design with sensitive groups to construct stimuli-responsive systems.[49] Stimuli, such as pH and light, and redox responsive organic components have been thoroughly studied.[72] Responses to pH and redox are widely exploited and realized by different organic components, especially in the tumor microenvironment.[73] For instance, poly(2-(diethylamino)ethyl methacrylate) (PDMAEMA) with hydrophilic/hydrophobic features under acidic/alkaline conditions, can be used as gatekeepers of nanohybrids for pH-responsive drug release.[74] Meanwhile, some small organic molecules may provide highly reactive moieties in the presence of stimuli. For example, introducing organic species with

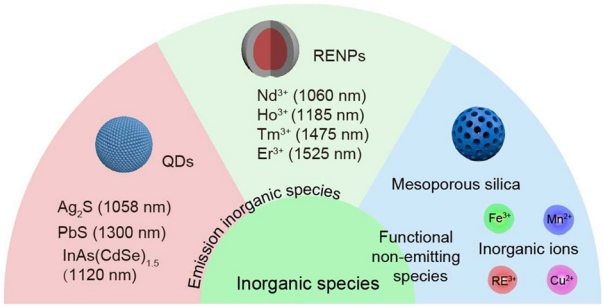

Fig. 4 The inorganic species, including emitting inorganic species (RENPs and QDs) and functional non-emitting species in NIR-II organic/inorganic nanohybrids. Adjustable NIR-II emission wavelength of RENPs can be obtained by doping different lanthanide ions, including Nd^{3+} (1060 nm), Ho^{3+} (1185 nm), Tm^{3+} (1475 nm) and Er^{3+} (1525 nm). Quantum dots (QDs) with different compositions have different maximum emission peaks, such as Ag_2S (1058 nm), PbS (1300), $InAs(CdSe)_{1.5}$ (1120 nm). Functional non-emitting species include mesoporous and inorganic ions.

disulfide bonds into nanohybrids is a strategy to realize redox responsiveness.[25] The implementation of multiple functions of nanohybrids can be realized by fusing multiple functional groups in organic species. Thus, the functional organic components will bring more opportunities for nanohybrid design.

2.2 Inorganic species

Inorganic species as building blocks for the construction of NIR-II nanohybrids can also be divided into two categories. One kind is NIR-II inorganic materials with NIR-II optical properties, including fluorescence emitting RENPs and QDs. The other kind is functional inorganic components without NIR-II emitting properties, such as mesoporous silica, metal ions, *etc.* (Fig. 4).

2.2.1 NIR-II inorganic materials. A wide range of NIR-II emitting inorganic materials provide diverse options for building organic/inorganic nanohybrids. Among them, RENPs[19] and QDs[75] are considered as ideal NIR-II inorganic materials.[76] Compared with the aforementioned organic dyes, NIR-II inorganic materials have relatively high QY, long-term photostability, as well as narrow-band and adjustable emissions. The adjustable NIR-II emission wavelength of RENPs can be obtained by doping different lanthanide ions, including Nd^{3+} (1060 nm and 1334 nm), Ho^{3+} (1185 nm), Pr^{3+} (1289 nm), Tm^{3+} (1475 nm) and Er^{3+} (1525 nm).[77] The emission peak width (30–50 nm) of RENPs is narrow, which is suitable for multiplex imaging. Meanwhile, RENPs have excellent photostability under physiological conditions, indicating the possibility of long-term monitoring of dynamic physiological processes. For example, Ho and Er-doped nanoparticles are able to achieve real-time multispectral NIR-II imaging of xenograft tumors.[78] QDs as the other class of NIR-II emitting inorganic materials also exhibit their excellent features, including high QY, large Stokes shift, and adjustable emission wavelength by controlling their size and shape. Ag_2S dots are NIR-II QDs that have been applied to monitor cell proliferation, organs and circulatory imaging, and real-time monitoring of the distribution of human mesenchymal stem cells.[79] Subsequently, several NIR-II QDs have been reported for blood vessel imaging and blood flow detection, including PbS, PbS-CdS, InAs, CdSe, and ZnSe QDs.[75] These NIR-II luminescent inorganic materials provide building blocks for the construction of NIR-II organic/inorganic hybrids.

2.2.2 Functional inorganic components without NIR-II optical properties. Besides NIR-II luminescence emitting materials, functional inorganic species without NIR-II optical properties, like silica nanoparticles, are also introduced as supporting skeletons to form nanohybrids with specific organic species.[80] Silica nanoparticles have been widely used in biomedical applications due to their controllable morphology, ease of surface functionalization, and good biocompatibility. Moreover, mesoporous silica with high specific surface area is suitable as a carrier for loading organic species such as drugs and dyes.[81,82] After loading into the mesopores, the optical properties of organic dyes will be altered due to the transformation from monomers to aggregates (including H-aggregates and J-aggregates), which will be discussed in Section 3.3. Inorganic ions, such as iron ions, rare earth ions, and copper ions, are another group of important functional inorganic materials. Ions can act as bridges to coordinate with organics, thus forming complexes with adjustable optical properties.

2.3 Fabrication strategies of NIR-II organic/inorganic nanohybrids

Different fabrication strategies have been reported for the construction of NIR-II organic/inorganic nanohybrids. Overall, there are two main methods, including surface functionalization and wrapping. Here, we briefly summarize the preparation methods of NIR-II nanohybrids, which may provide reference for designing more ideal nanohybrids in the future.

Surface functionalization on inorganic species is the most common method to fabricate NIR-II nanohybrids. The amphiphilic functional polyethylene glycol (PEG)-phospholipids are powerful to endow nanohybrids with good biocompatibility and functionality.[19] For example, the oleic acid-encapsulated RENPs can be modified with amine–PEG–phospholipid on a hydrophobic surface through van der Waals interaction.[83] And the amino group provides a reactive site for subsequent modifications. Carboxyl or thiol group-terminal PEG or lipids have also been successfully attached to inorganic species, which provides an opportunity to construct NIR-II nanohybrids.[65] Meanwhile, click chemistry with a high reaction yield provides a reliable and convenient approach that has been used to fabricate different NIR-II nanohybrids.[84] Organic species with some special groups can directly coordinate with inorganic species to form NIR-II nanohybrids.[85] For instance, GSH with two carboxyl groups has been modified on RENPs to form NIR-II nanohybrids with good biocompatibility and functionality.[25]

Wrapping is another fabrication strategy to build NIR-II nanohybrids *via* noncovalent interaction between organic and inorganic species. Mesoporous inorganic species with large surface area are suitable for carrying organic species through direct precipitation methods. For example, IR-140[82] and FD-1080[81] fluorophores can enter the cavity of mesoporous silica

through hydrophobic or electrostatic interaction to form J-aggregation in nanohybrids for NIR-II bioimaging. In another case, hydrophobic dyes easily encapsulated into the PEG layer on inorganic nanoparticles surface *via* hydrophobic interaction, such as NIR-II nanohybrids composed of MY-1057 and RENPs.[49] These approaches not only integrate organic and inorganic species, but also offer great opportunities to tune the properties of nanohybrid materials by regulating inorganic and organic species.

2.4 Property and function of NIR-II organic/inorganic nanohybrids

Through the combination of organic and inorganic species, nanohybrids can create new properties including the size, morphology, surface properties, and optical properties, which are crucial in the design of potentially useful nanohybrids for biomedical applications. Thus, an in-depth understanding of the properties and functions of nanohybrids is of great importance when looking into the relationship between structures, properties, and performances. In this subsection, NIR-II organic/inorganic nanohybrids for biomedical applications are categorized in two parts: (1) the nanohybrids realize their new features based on the function of single species (organic or inorganic); (2) the nanohybrids realize their new features through the interaction between organic and inorganic species. The morphology, assembly/disassembly, and optical properties of nanohybrids are summarized to motivate the development of nanohybrids with better performances.

When the nanohybrids realize their new features based on the individual species, the function of the organic or inorganic component is critical for the nanohybrids. Integrating organic or inorganic components with various responsive moieties (such as pH or redox sensitive groups) into nanohybrids can be used for the detection or treatment of related diseases.[72,86,87] Self-assembly or disassembly of NIR-II organic/inorganic nanohybrids can be implemented by introducing functional or stimulus-responsive organic species (Fig. 5A). New properties and functions can be generated by designing stimulus-responsive nanohybrids. Typically, functional organic species can realize self-assembly of nanohybrids by host–guest interactions, bio-recognition, and stimulus-responsive crosslinking. For example, GSH with redox characteristics can be modified to the surface of inorganic components with an exposed sulfydryl.[25] In the presence of ROS at lesions, nanohybrids can specifically crosslink to form clusters due to the formation of disulfide bonds between organic species. The formation of aggregation at the lesion can increase the accumulation of nanohybrids and improve the imaging signal intensity. Moreover, the aggregation with large volume shows long retention at lesions, which extends the imaging time window due to a slow excretion rate. Furthermore, external stimuli, such as light and temperature, could trigger the disassembly of aggregates in specific sites, achieving the rapid excretion *in vivo*.[68] On the other hand, many inorganic materials with high specific surface area are suitable as carriers for loading organic species, which may induce unique properties, such as dye aggregates with bathochromic or hypochromatic shifted absorbance and emission peaks compared to monomers (Fig. 5B). For instance, mesoporous silica as nanocarriers has been used to induce and stabilize J-aggregates formed by cyanine dyes.

In other NIR-II nanohybrids, unique synergistic properties, especially optical properties, are generated based on interaction between organic and inorganic species. The transfer process of photons between organic and inorganic species provides an opportunity to design a variety of sensing mechanisms or strategies for different biomedical applications, including FRET, dye sensitizing methods, secondary absorption, ACIE, and dual emitting systems (Fig. 5C–H). The synergistic properties between organic and inorganic components of nanohybrids based on the above mechanisms will be discussed in detail in Section 4. In general, inorganic species, such as RENPs and QDs, have robust optical properties, which are suitable to serve as donors in energy transfer systems or reference signals in ratiometric fluorescence systems.[8] In contrast, organic species, such as polymethine dyes with flexible structural modification, stimuli responsiveness, or relatively weak structural stability, are suitable to act as responsive signals.[8] Based on energy transfer, dye sensitizing methods, secondary absorption, ACIE strategy, and dual emitting systems, nanohybrids can be constructed to detect analytes. In addition, FRET based nanohybrids can also be used as probes for fluorescence (or luminescence) lifetime imaging and sensing.[49,88]

Versatile NIR-II organic/inorganic nanohybrids based on functional organic and inorganic species provide the possibility to not only realize a combination of functions, but also create new diversities and more responsiveness for biomedical applications, which will be discussed in detail in the next two sections.

3. NIR-II nanohybrids based on functional organic/inorganic species for enhancing performance

In nanohybrids consisting of the NIR-II emitter and functional components without NIR-II optical properties, the functional components could regulate the optical performance of the nanohybrids through recognition or responsiveness. This section will be divided into three parts: (i) organic recognition induced nanohybrid aggregation; (ii) responsive organic component induced nanohybrid assembly and disassembly; (iii) inorganic component mediated organic molecular J-aggregates formation.

3.1 Organic recognition induced nanohybrid aggregation

Since the surface of inorganic components can be modified with organic species, inorganic components can be used as scaffolds to design nanohybrids for biomedical applications. Nanohybrids are convenient platforms due to the surface multifunctional modification and large specific surface area.[89] Functional organic species of NIR-II nanohybrids based on host–guest recognition and bio-recognition are the most

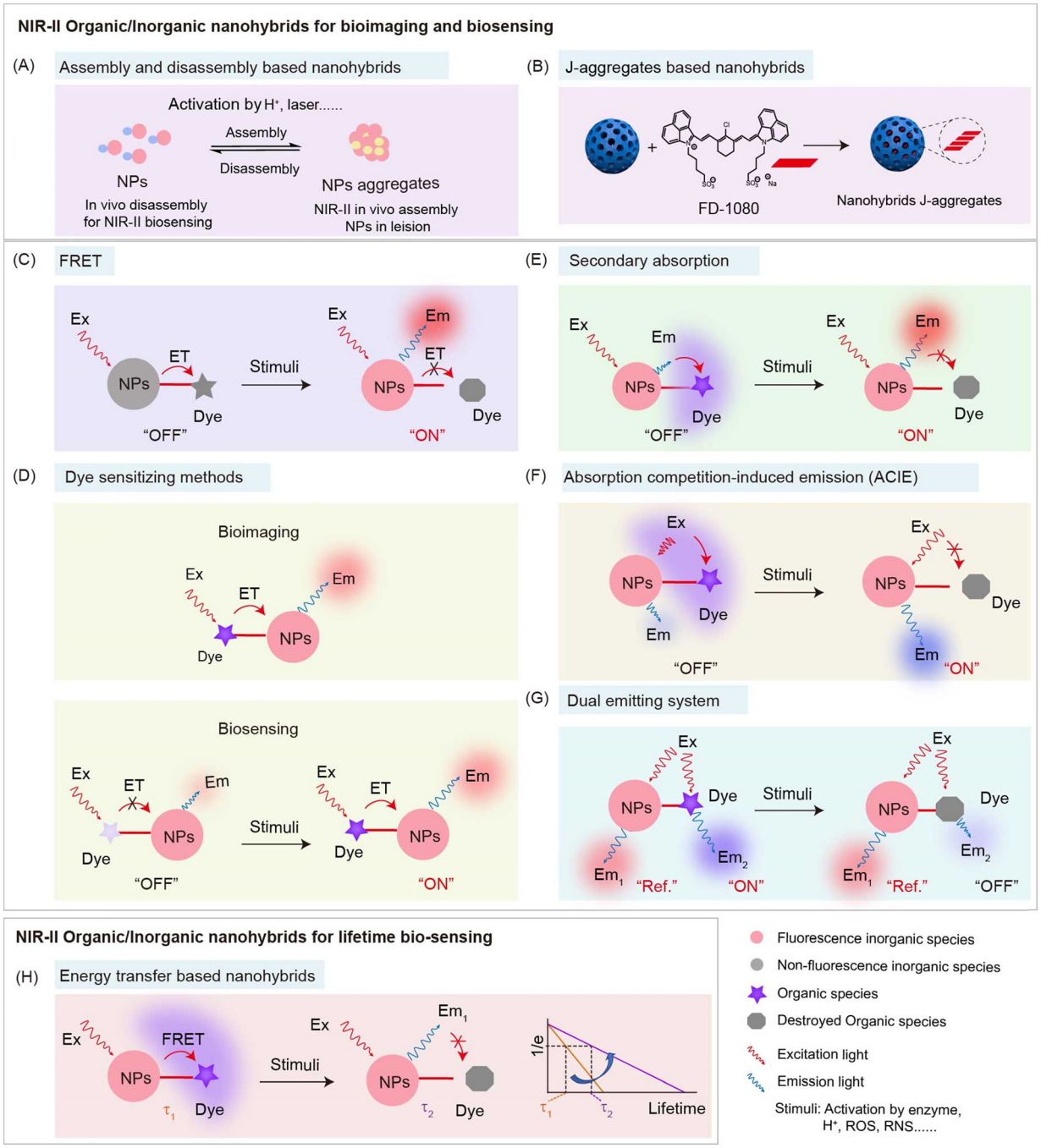

Fig. 5 The overview of mechanism of NIR-II organic/inorganic nanohybrids for intensity-based and lifetime-based bioimaging and biosensing, including assembly and disassembly between nanohybrids (A), forming J-aggregates based nanohybrids (B), energy transfer (C and H), dye sensitizing methods (D), secondary absorption (E), absorption competition-induced emission (ACIE) (F), and dual emitting system (G).

widely utilized approaches to fabricate smart systems for biomedical applications.

Although *in vivo* NIR-II bio-imaging has shown advantages of high resolution with deeper penetration, the low specific accumulation of NIR-II probes at lesions still leads to a low signal-to-noise ratio (SNR), which is mainly due to the high capture by the mononuclear phagocyte system (MPS) after intravenous (i.v.) injection into animals.[90] Thus, smart systems with high accumulation at the lesion site and less capture by MPS to improve the imaging SNR is of urgent need. *In vivo* assembly and disassembly of probes have been developed to increase SNR at lesions. Introducing small organic groups with spontaneous recognition, such as the host–guest interaction, and DNA base pairing, into hybrids systems is also suitable for this purpose (Fig. 6A).[91]

The complementary base pairing of DNA is the fundamental law of nature's genetic materials, whose high specific recognition provides an ideal tool as a surface ligand to trigger *in vivo*

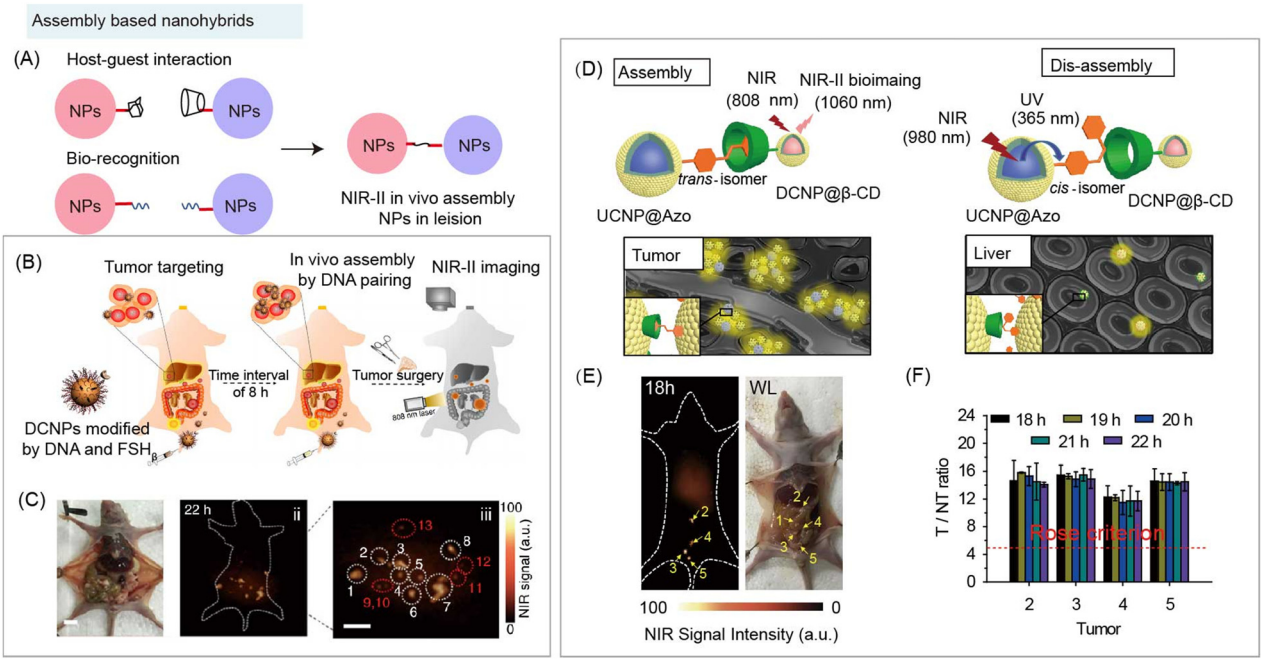

Fig. 6 Assembly based organic/inorganic nanohybrids for NIR-II bio-imaging. (A) Schematic of nanohybrids for *in vivo* aggregation based on organic specific recognition. (B) Schematic of assembly based nanohybrids containing DNA and DCNPs for NIR-II bioimaging guided surgery. (C) Optical photo and NIR-II bioimaging of human ovarian adenocarcinoma peritoneal metastases model after injecting nanohybrids. Reproduced with permission from ref. 83, copyright 2018, Springer. (D) Schematic of host–guest induced assembly at tumor and NIR laser-regulated disassembly at liver of nanoprobes containing azobenzene (Azo) modified UCNPs and β-CD modified DCNPs for NIR-II bioimaging. (E) NIR-II bioimaging and optical photo of human ovarian adenocarcinoma peritoneal metastases model after nanohybrids based *in vivo* assembly and disassembly strategy. (F) T/NT ratios of tumors at different times. Reproduced with permission from ref. 19, copyright 2018, Wiley-VCH.

aggregation of inorganic nanoparticles. Nanohybrids containing DNA and Nd^{3+} doped downconversion nanoparticles (DCNPs) were constructed as imaging probes for *in vivo* assembly (Fig. 6B).[83] After DNA recognition, nano-aggregation within the size of 100–500 nm was formed at the tumor site and the accumulation content reached 17.5%ID g^{-1} (percent of injected dose per gram), leading to the high SNR (SNR > 11) during NIR-II imaging in the human ovarian adenocarcinoma peritoneal metastases tumor bearing mouse model (Fig. 6C).

In addition, reversible and controllable supramolecular recognition also exhibits its potential to improve the NIR-II imaging SNR by increasing contrast agent accumulation at lesions and decreasing capture by MPS. Zhang and coworkers developed an efficient *in vivo* assembly through β-cyclodextrin–azobenzene (β-CD–Azo) recognition at the tumor site to increase probe accumulation. Meanwhile, 980 nm NIR light was applied to mediate disassembly at the liver site to reduce the background signal and improve the SNR of NIR-II bioimaging (Fig. 6D).[19] β-CD modified Nd^{3+} doped downconversion nanoprobes (DCNP@β-CD) and azobenzene modified Tm^{3+} doped upconversion nanoparticles (UCNP@Azo) were sequentially i.v. injected into subcutaneous tumor-bearing mice. After assembly through host–guest interaction between the two nanohybrids, nanoaggregates were formed at the tumor site, leading to an increased signal and accumulation (9.97 ± 0.60%ID g^{-1}). Under 980 nm laser irradiation, the UCNPs emitted ultraviolet (UV) and blue light at 365 and 475 nm, which were capable of triggering transformation of the azo group between *trans* and *cis* configurations, and then inducing disassembly of nanohybrids in the liver. Therefore, during NIR-II tumor imaging, the NIR light-regulated assembly/disassembly strategy exhibited a low background signal, leading to a high tumor-to-liver ratio (2.62 ± 0.22) and SNR (SNR > 15). Then, the authors studied the potential application using this strategy for surgical excision of peritoneal metastatic human ovarian adenocarcinoma under NIR-II image guidance (Fig. 6E), NIR-II imaging showed a high tumor SNR (SNR > 10) and a tumor-to-liver ratio (1.5–3.0) (Fig. 6F).

These results demonstrated that two goals can be achieved by the *in vivo* assembly and disassembly strategy. One is that the nanohybrids would specifically crosslink at lesions, increasing the accumulation by enlarging the size, which would enhance the signal intensity at lesions. The other goal achieved is that the *in vivo* disassembly strategy can be used to reduce the amount of nanohybrids deposited in normal tissues, which would decrease the background signal in normal tissue. These flexible assembly and disassembly strategies enable the fabrication of multifunctional nanohybrids by integrating functional organic species for enhanced NIR-II bioimaging and biosensing.

3.2 Responsive organic components induced stimuli-activated assembly and disassembly of nanohybrids

NIR-II organic/inorganic nanohybrids can be used not only for bio-imaging but also for the detection of some biological substances, such the acidic microenvironment, ROS, RNS, *etc.*

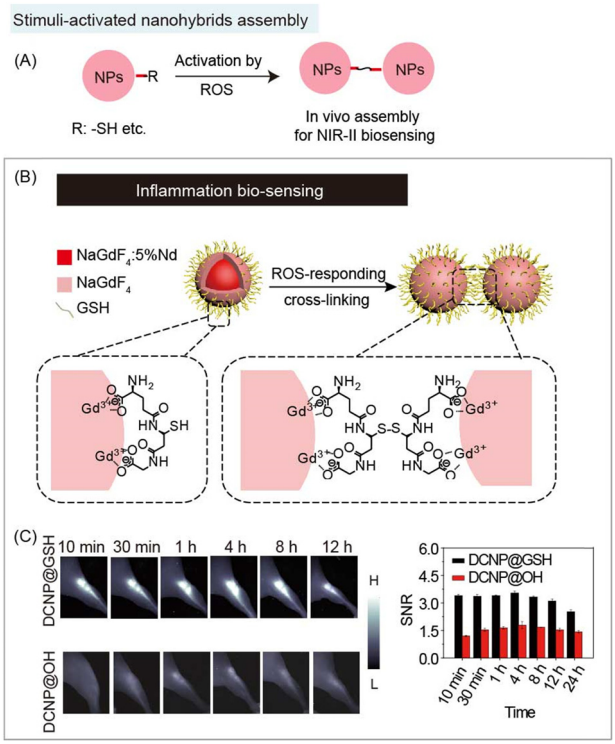

Fig. 7 Responsive organic molecules for nanohybrid aggregation during NIR-II biosensing. (A) Schematic of responsive organic based aggregation of nanohybrids. (B) Schematic of cross-link induced aggregation of glutathione modified DCNP nanohybrids for NIR-II acute local epidermal inflammation bio-detection. (C) NIR-II imaging (left) and SNR (right) of the acute local epidermal inflammation with nanohybrids. Reproduced with permission from ref. 25, copyright 2019, Wiley-VCH.

The NIR-II bio-sensing for analytes can be realized by utilizing the responsive organic components.

The principle of aggregation/disaggregation (or assembly/disassembly) based nanohybrids is that the analytes can trigger size changes of nanohybrids (Fig. 7A and 8A). For example, ROS, such as hydroxyl radical ($OH^{\bullet -}$), and hydrogen peroxide (H_2O_2), as analytes have been used in *in vivo* assembly of inorganic nanoparticles.[25] Typically, GSH modified ultrasmall DCNP (DCNPs@GSH) nanohybrids can respond to ROS for acute local epidermal inflammation bio-sensing (Fig. 7B).[25] The exposed sulfhydryl group of organic components, GSH, could be oxidized by ROS to form a disulfide bond, leading to the aggregation of nanohybrids at the inflamed area. After *in vivo* aggregation, NIR-II bioimaging at inflammation lesions has a high SNR of 3.5, which is 2.9 times higher than that of the control group (hydroxy modified DCNPs) (Fig. 7C).

Besides the assembly/disassembly of "always on" NIR-II nanohybrids, there is another "off–on" strategy for NIR-II biosensing. In these aggregates, fluorophores and quenchers aggregate based on the coordination and hydrophobic interactions. Due to FRET or secondary absorption between fluorophores and quenchers, the fluorescence signal would remain "off". Under stimuli, disaggregation would be triggered to "turn on" the fluorescence signal (Fig. 8A). In addition, nanohybrids with *in vivo* assembly/disassembly features can not only realize the

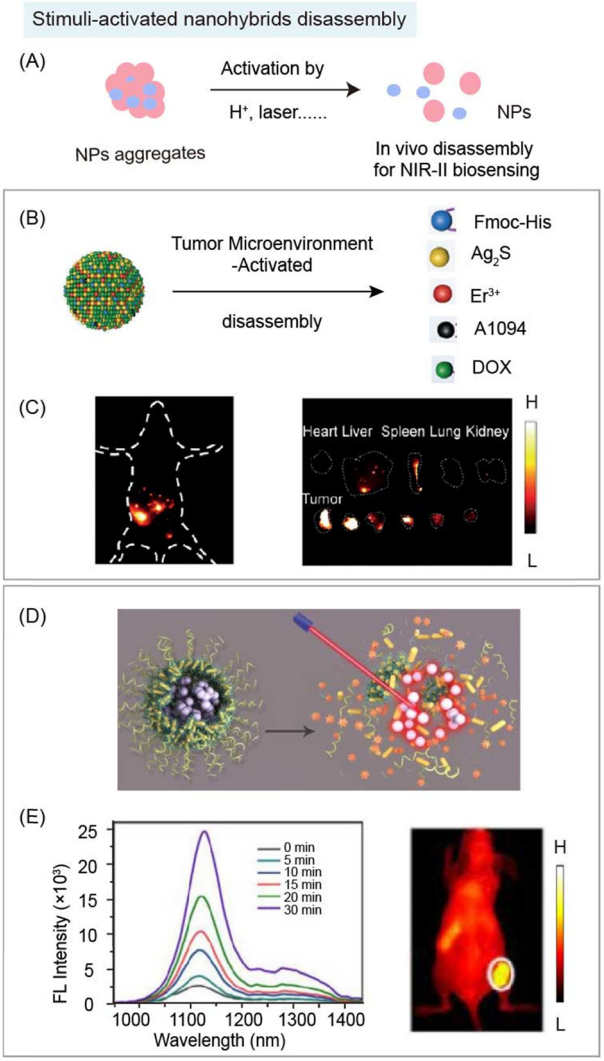

Fig. 8 Responsive organic molecules for nanohybrid disaggregation during NIR-II biosensing. (A) Schematic of stimulus (*e.g.* enzyme, H^+, laser *etc.*) responsive organic molecule-based nanohybrids for disaggregation during NIR-II biosensing. (B) Schematic of acidic tumor microenvironment induced disaggregation of nanohybrids containing Fmoc-His, Er^{3+}, Ag_2S, DOX, and NIR-II dye A1094 for NIR-II detection of peritoneal metastatic tumor. (C) NIR-II whole-body image (left) and *ex vivo* organs and tumor image (right) after the administration of nanohybrids. Reproduced with permission from ref. 85, copyright 2020, Wiley-VCH. (D) Schematic of NIR light induced disaggregation of nanohybrids containing gold nanorods, light-responsive polyprodrug PolyRu, NIR-II dye IR1061 for NIR-II bioimaging guided cancer synergistic chemo-PDT cancer therapy. (E) Emission spectra of nanohybrids under 808 nm laser irradiation with different periods of time (left). NIR-II tumor image of MCF-7 tumor bearing mice with nanohybrid administration (right). Reproduced with permission from ref. 92, copyright 2020, Ivyspring International Publisher.

detection of analytes, but also combine therapeutic properties of organic or inorganic components for diagnosis and treatment. Wang and coworkers reported acidic tumor microenvironment (TME) induced disaggregation of nanohybrids containing Fmoc-His, Er^{3+}, Ag_2S QDs, chemotherapeutics doxorubicin (DOX), and NIR-II quencher A1094 for detection and therapy of peritoneal metastatic tumors (Fig. 8B).[85] Through breaking intermolecular

forces, including metal coordination and hydrophobic interactions, nanohybrids would disaggregate in response to the acidic TME, decreasing the quenching effect of A1094 to turn on the NIR-II fluorescence signal of Ag_2S QDs (SNR > 5), and releasing DOX within the tumor to realize chemotherapy (Fig. 8C). Besides the TME responsive disassembly, laser mediated disassembly was also developed by Song and coworkers with spatiotemporally controllable drug release. The inorganic quencher gold nanorods, NIR-II organic emitter dye IR1061, and light-responsive polyprodrug (polyRu) were assembled through hydrophobic interactions. 808 nm NIR light was used to trigger the release of the Ru drug and change the hydrophobicity of the polymer, leading to the disaggregation (Fig. 8D). The turn-on NIR-II signal achieved the NIR-II bioimaging guided synergistic chemo-photodynamic cancer therapy (Fig. 8E).[92] These aggregated nanohybrids are promising platforms to realize multifunction for *in vivo* NIR-II bio-sensing and disease therapy.

3.3 Inorganic component mediated organic molecular J-aggregates formation

NIR-II organic molecules are commonly used as contrast agents during bioimaging and biosensing. Interestingly, their optical properties could be entirely different after ordered aggregation. For instance, J-aggregates are formed by a highly ordered head-to-tail arrangement of individual molecules.[93] Compared with monomers, J-aggregates have excellent photophysical properties, such as red-shifted absorption and emission bands, enhanced absorption coefficients, and so on. J-aggregates could be induced by some inorganic skeletons. Mesoporous silica with flexible surface functionalization, porous structure, and controlled morphology is considered as an excellent carrier for biomedical applications. Surprisingly, the porous structures could not only load the organic molecules, but also induce the ordered aggregation of organic molecular dyes.

Nanohybrids formed from organic dyes, especially polymethine dyes, induced by some inorganic components (Fig. 9A). Sletten and co-workers reported that J-aggregates NIR-I dye IR-140 (Abs./Em.: 862/875 nm) were formed inside hollow mesoporous silica nanoparticles (HMSNs) (Fig. 9B).[82] IR-140 J-aggregates showed two different forms of aggregates in the absorption spectrum, J1-aggregates (Abs./Em.: 965 nm/non-emission), and J2-aggregates (Abs./Em.: 1040/1047 nm). Zhang and co-workers also developed FD-1080 J-aggregates (Abs./Em.: 1360/1370 nm) formed by self-assembly of 1,2-dimyristoyl-*sn*-glycero-3-phosphocholine (DMPC) and cyanine dye FD-1080.[94] The same group also found that FD-1080 can be loaded and induced into mesoporous silica coated titanium plates (MSTPs) to form FD-1080 J-aggregates for NIR-II imaging guided osteosynthesis (Fig. 9C-E).[81] Beyond all doubt, J-aggregate based nanohybrids are a new class of NIR-II probes for bioimaging or biosensing in a broad region. Inorganic materials may provide a method to obtain the aggregates, and nanohybrids can be constructed by fully exploring the properties of existing organic species and combining with inorganic species.

4. Interaction between organic and inorganic species of NIR-II nanohybrids for enhancing the performance

This part will discuss the unique optical properties of NIR-II organic/inorganic nanohybrids based on interactions between organic and inorganic species to achieve intensity and lifetime

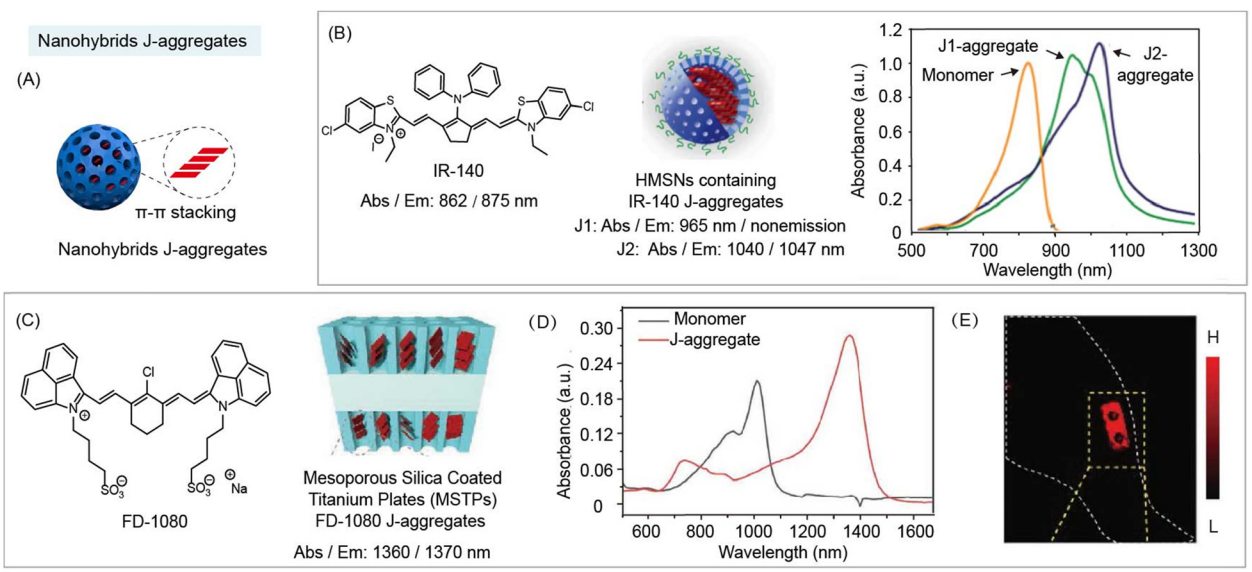

Fig. 9 NIR-II nanohybrid J-aggregates for bioimaging and biosensing. (A) Schematic of J-aggregate based nanohybrids for NIR-II bio-imaging. (B) Chemical structure of IR-140 (left). Schematic of nanohybrid J-aggregates containing IR-140 and hollow mesoporous silica nanoparticles (middle). Absorption spectra of nanohybrid J-aggregates (right). Reproduced with permission from ref. 82, copyright 2019, American Chemical Society. (C) Chemical structure of FD-1080 (left). Schematic of nanohybrid J-aggregates containing FD-1080 and mesoporous silica coated titanium plates (MSTPs) (right). (D) Absorption spectra of monomer and nanohybrid J-aggregates. (E) NIR-II images *in vivo* implantation of nanohybrid J-aggregates at mice hindlimb. Reproduced with permission from ref. 81, copyright 2021, Wiley-VCH.

bioimaging and biosensing. The interactions between organic and inorganic components will be mainly summarized into four parts: FRET, dye sensitizing methods, secondary absorption, and ACIE. Interestingly, the energy transfer between organic and inorganic components can not only alter the fluorescence (or luminescence) intensity, but also affect the fluorescence (or luminescence) lifetime of the energy donor and acceptor, which could be used for fluorescence (or luminescence) intensity and lifetime biosensing.

Most commonly, researchers tend to modify organic molecular dyes into single inorganic nanoparticles to construct nanohybrids to realize NIR-II bioimaging and bio-sensing. As mentioned above, organic components, such as IR-1061, MY-1057, and FD-1080 with high absorption coefficients and high fluorescence emission could be used as both fluorophores and quenchers.[49,95] Organic species with flexibly designed responsive moieties are easily stimulated by the analytes to change their spectral characteristics. In contrast, inorganic components, such as QDs and RENPs, with robust emission features, are hardly used as probes for bio-sensing themselves. Nevertheless, they are suitable as energy donors and reference signals owing to their stable spectral properties.[8] Based on an in-depth understanding of design mechanism, an optimized NIR-II nanohybrid can be designed and fabricated for diverse functions and enhanced performances.

4.1 FRET based nanohybrids

Energy transfer is an electrodynamic phenomenon that occurs between a donor in the excited state and an acceptor in the ground state. Energy transfer without the emission and reabsorption of a photon is an energy exchange process based on long range dipole–dipole interaction with a similar resonance frequency between the donor and acceptor. The rate of energy transfer is related to the following aspects: the extent of overlap between the emission spectrum of the donor and absorption spectrum of the acceptor (the acceptor is not required to have the characteristic of fluorescence emission); the relative orientation of the donor and the acceptor transition dipoles; the QY of donor; the distance between the donor and acceptor. Here are some points of energy transfer that should be noted: (1) there is no photon in the energy transfer process, (2) the energy transfer is not a process where photons emitted by the donor are absorbed by the acceptor, and (3) the energy transfer between the donor and acceptor is through dipole–dipole interactions.

Controllable energy transfer between organic and inorganic species in the NIR-II region could be achieved through a suitable selection of components in the nanohybrids. Among energy transfer based nanohybrids, inorganic species are often used as FRET donors, and organic species with responsive optical changes can be used as FRET acceptors (Fig. 10A). Thus, the optical characteristics usually stem from inorganic species of NIR-II nanohybrids. For example, Wang and coworkers developed FRET nanohybrids system V&A@Ag_2S containing Ag_2S QDs (as the donor), and NIR-II dye A1094 (as the acceptor) for real-time vascular inflammation biosensing (Fig. 10B).[50] Upon addition of $ONOO^-$, the NIR-II fluorescence intensity of Ag_2S QDs increased along with the destruction of A1094 (Fig. 10C). Thus, energy transfer based nanohybrids can achieve NIR-II vascular inflammation biosensing with a high SNR (SNR = 10.2) in the traumatic brain injury mouse model (Fig. 10D). Similarly, RENPs could also be used as an energy donor in nanohybrids. Mei and coworkers reported an energy transfer system containing RENPs (donor) coated with mesoporous silica and NIR-II dye FD-1080 (acceptor) for the detection of ClO^- in raw milk (Fig. 10E).[96] After reacting with ClO^-, the NIR-II fluorescence intensity of nanohybrids recovered due to the destruction of FD-1080 (Fig. 10F and G). Besides monomers, dye aggregates could also serve as an energy acceptor. Zhang and coworkers reported an energy transfer system using Nd^{3+} and Er^{3+}-doped RENPs as donors, and NIR-II FD-1080 J-aggregates as acceptors for ClO^- sensing (Fig. 10H).[97] FD-1080 J-aggregates exhibit a maximum absorption wavelength at 1360 nm, which overlaps well with the Nd^{3+} emission at 1330. Energy transfer from Nd^{3+} to FD-1080 J-aggregates was observed by the decrease of a lifetime (173 μs to 51 μs) at 1330 nm under 808 nm excitation. Meanwhile, FD-1080 J-aggregates were sensitive to ROS. Thus, by utilizing the Er^{3+} 1550 nm emission as a reference signal, the nanohybrids exhibited a ratiometric response for ClO^- in lipopolysaccharide (LPS)-treated mice (Fig. 10I). These multifunctional organic/inorganic nanohybrids provide new ideas for the design of nanohybrids with tunable properties and related functions.

4.2 Dye sensitizing methods based nanohybrids

In addition to the above-mentioned energy transfer from inorganic to organic species, there is also an energy transfer pathway from organic to inorganic species. Dye sensitized nanohybrids are designed to generate the enhanced fluorescence (or luminescence) emission for imaging and sensing by direct non-radiative energy transfer from excited states of organic species to inorganic species (Fig. 11A).[62,64,98,99] Due to their abundant 4f energy level configuration, RENPs with narrow (~10 nm) and small absorption cross section (~10^{-20} cm^{-2}), and nonblinking narrow band emission are widely used as inorganic species in this strategy.[19] Organic species are generally cyanine dyes with a large absorption cross section (10^{-16} cm^{-2} for ICG), which act as light harvesting antenna.[100] Thus, dye sensitized nanohybrids provide a way to solve the performance-limiting problem, generating multifold brightness higher than that of RENPs without dye sensitization. Prasad and coworkers reported dye sensitized nanohybrids consisting of $NaYF_4$:Yb^{3+}/X^{3+}@$NaYbF_4$@$NaYF_4$:Nd^{3+} (X = null, Er, Ho, Tm, or Pr) and the organic dye, ICG, attached to the surface (Fig. 11B and C).[62] This nanohybrid can produce enhanced (~4-fold) multicolor narrow-band emissions (1000 nm for Yb^{3+}, 1165 nm for Ho^{3+}, 1310 nm for Pr^{3+}, 1460 nm for Tm^{3+}, and 1530 nm for Er^{3+}) with a large Stokes shift (>200 nm), by direct non-radiative energy transfer from the light-harvesting surface of ICG to emitter X^{3+} in the core (Fig. 11D). Then, a sharp NIR-II image of injection point through 3 mm mouse tissue was observed after subcutaneous injection of ICG-sensitized Er^{3+}-doped nanohybrids (Fig. 11E). Meanwhile, Li

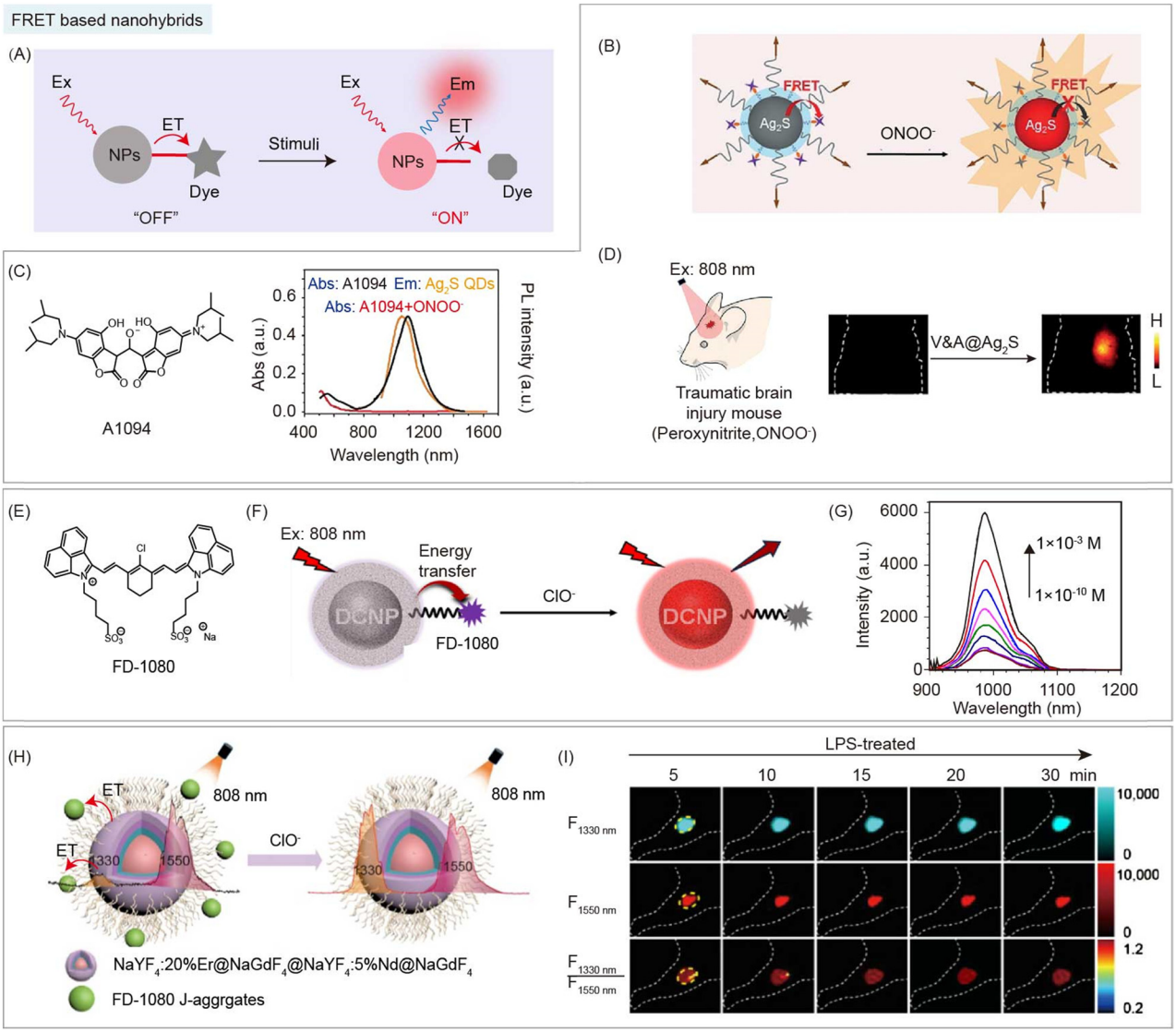

Fig. 10 FRET based organic/inorganic nanohybrids for NIR-II biosensing. (A) Schematic of FRET based nanohybrids after stimulation by enzymes, H^+, ROS, RNS, *etc.* for NIR-II bio-sensing. (B) Schematic of the FRET system of nanohybrid V&A@ Ag_2S containing Ag_2S (donor), and NIR-II dye A1094 (acceptor) for $ONOO^-$ detection. (C) Chemical structure of A1094 (left). Absorption and emission spectra of nanohybrids in response to $ONOO^-$ (right). (D) NIR-II imaging of the traumatic brain injury model after nanohybrids V&A@ Ag_2S administration. Reproduced with permission from ref. 50, copyright 2019, Wiley-VCH. (E) Chemical structure of FD-1080. (F) Schematic of the energy transfer system of nanohybrids containing RENPs (donor), and NIR-II dye FD-1080 (acceptor) for ClO^- detection. (G) Recovery of the emission spectra of nanohybrids in response to ClO^-. Reproduced with permission from ref. 96, copyright 2021, American Chemical Society. (H) Schematic of FRET nanohybrids containing Nd^{3+} and Er^{3+}-doped RENPs (donor), and NIR-II FD-1080 J-aggregates (acceptor) for ClO^- detection. (I) NIR-II images and corresponding ratiometric images of LPS-treated mouse at different time points after nanohybrid administration. Reproduced with permission from ref. 97, copyright 2022, Chinese Chemical Society.

and coworkers developed dye sensitized nanohybrids containing dye, ALK-pi, and Er^{3+}-doped RENPs with boosted NIR-IIb emissions (Fig. 11F).[63] Thanks to ~40-fold enhanced brightness *via* Alk-pi sensitization, the NIR-II vascular network of mice with high spatial resolution can be observed (Fig. 11G).

Besides, the above mechanism interpretation may shed light on the design of stimuli-responsive dye sensitized nanohybrids as promising contrast agents. In general, light-harvesting dyes are designed as responsive groups, allowing nanohybrids for NIR-II biosensing (Fig. 11H). Song and coworkers reported dye sensitized nanohybrids containing GSH-responsive cyanine dye, NPh, and Er^{3+}-doped RENPs for NIR-II bioimaging of orthotopic colorectal cancer mice (Fig. 11I).[64] NPh reacted with GSH to form Cy7-SG with a high QY, leading to the turn-on luminescence of nanohybrids at 1550 nm under 808 nm excitation *via* non-radiative energy transfer from Cy7-SG to emitter Er^{3+}-doped RENPs. However, under 980 nm excitation, the luminescence intensity of nanohybrids at 1550 nm remains unchanged due to the negligible absorbance of Cy7-SG at 980 nm. Thus, the ratiometric emission intensity at 1550 nm with 808 nm and 980 nm excitation can be used for GSH detection and NIR-II ratiometric bioimaging (Fig. 11J).

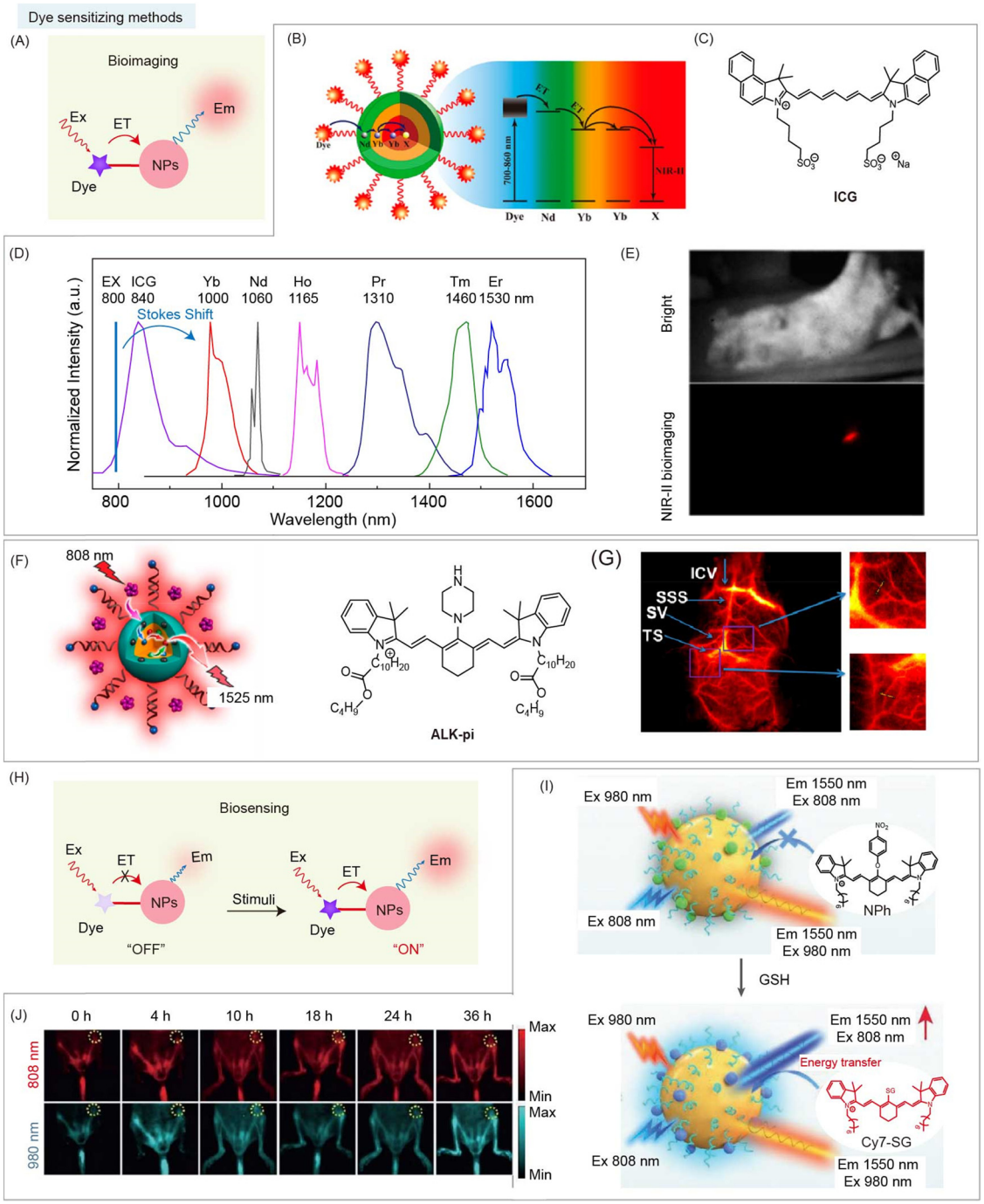

Fig. 11 Dye sensitizing method based NIR-II organic/inorganic nanohybrids for bioimaging and biosensing. (A) Schematic of dye sensitizing method based NIR-II nanohybrids for bioimaging. (B) Schematic of dye sensitized nanohybrids and energy transfer pathway from ICG to RENPs. (C) Chemical structure of ICG. (D) Normalized multichannel NIR-II emission spectra from nanohybrids with different lanthanide ions. (E) NIR-II fluorescence imaging of a mouse after subcutaneous injection of ICG-sensitized Er^{3+}-doped nanohybrids (excited at 800 nm). Reproduced with permission from ref. 62, copyright 2016, American Chemical Society. (F) Schematic of dye sensitized nanohybrids with energy transfer from organic dye Alk-pi to RENPs. (G) NIR-II brain vascular imaging and the corresponding magnified images using Alk-pi-sensitized nanohybrids. Reproduced with permission from ref. 63, copyright 2021, American Chemical Society. (H) Schematic of dye sensitizing method based NIR-II nanohybrids after stimulation for NIR-II bio-sensing. (I) Schematic of dye sensitized nanohybrids for ratiometric detection of GSH and tumor bioimaging. (J) NIR-II bioimaging of orthotopic colon cancer with nanohybrid administration under 808 nm and 980 nm laser illumination at different time points, respectively. Reproduced with permission from ref. 64, copyright 2021, Wiley-VCH.

Dye sensitizing methods are designed to improve the emission intensity of RENPs, which mainly alleviates the problem of insufficient light harvesting. By integrating the advantages of large absorption cross-sections of organic dyes and abundant

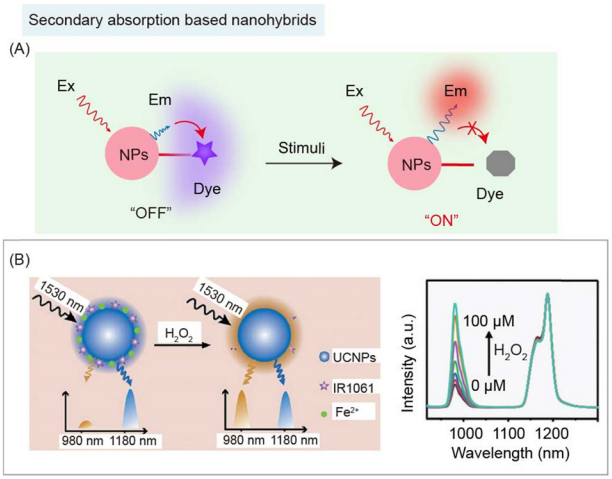

Fig. 12 Secondary absorption based NIR-II organic/inorganic nanohybrids for biosensing. (A) Schematic of secondary absorption based nanohybrids before and after stimulation for NIR-II bio-sensing. (B) Schematic of ratiometric nanohybrids containing UCNPs and NIR-II dye IR1061 for detection of H_2O_2 (left). Recovery of H_2O_2 responsive emission spectra of nanohybrids (right). Reproduced with permission from ref. 95, copyright 2018, Wiley-VCH.

energy levels of RENPs, nanohybrids with high brightness and tunable emission wavelengths are available. Meanwhile, stimulus-responsive dyes as antenna endow nanohybrids with sensing ability in the NIR-II region.

4.3 Secondary absorption based nanohybrids

In some cases, if the distance between inorganic and organic components is too far to have an energy transfer process happen, organic species with a high absorption coefficient can still be used as a photon filter layer to absorb the emission of inorganic species, which is known as secondary absorption, causing the nanohybrid's fluorescence (or luminescence) signal intensity to change (Fig. 12A). Both energy transfer and secondary absorption between organic and inorganic species will cause absorption and emission spectral changes. However, the fluorescence (or luminescence) lifetime variation of the donor and acceptor will only occur during the energy transfer, but not during the secondary absorption process. Zhang and coworkers reported a secondary absorption based nanohybrid containing Er^{3+} sensitized RENPs with 980 and 1180 nm emissions under 1530 nm excitation.[95] NIR-II dye IR1061 was used as an H_2O_2 responsive filter to absorb emission at 980 nm. Upon addition of H_2O_2, the emission at 980 nm of the nanohybrids recovered along with decomposition of IR1061. Meanwhile, the emission at 1180 nm of RENPs remained unaltered, which served as a stable reference signal for NIR-II ratiometric biosensing of epidermal inflammation (Fig. 12B). In a secondary absorption system, there is no strict requirement for the distance between emitters and absorbers. Thus, this strategy could be used in larger scaled devices, such as microneedles and 3D printed devices.

4.4 ACIE based nanohybrids

Compared with lanthanide ions, organic species have a higher absorption coefficient (usually 10^3 times higher), making them an efficient absorption layer to absorb not only emission light, but also excitation light. Therefore, nanohybrids composed of organic species with high absorption coefficient and inorganic species with low absorption coefficient become competitors towards laser excitation, which was reported as ACIE.[66] RENPs are widely used as inorganic species in this strategy, due to their multi-excitation bands, low absorption coefficients, and narrow emission spectra. For instance, Nd^{3+}-doped RENPs can emit fluorescence at 1064 nm under both 730 and 808 nm laser excitations, and Er^{3+}-doped RENPs have emissions at 1525 nm under 808 and 980 nm laser excitations.[66] Stimulus-responsive organic dyes are well suited as competition absorbers for absorbing one of the excitation wavelengths. On the other hand, the stable fluorescence signal of RENPs under another excitation wavelength can be utilized as a reference signal. Thus, stimulus-responsive organic species of nanohybrids serve as photon filtration layers affecting only one excitation wavelength, achieving ratiometric NIR-II bioimaging or biosensing (Fig. 13A). Based on this mechanism, Zhang and coworkers reported ACIE nanohybrids containing DCNPs and NIR dye NPTAT for monitoring gastrointestinal drug release (Fig. 13B).[66] NIR dye, NPTAT, with a maximum absorption of around 625 nm was used as an absorbing competitor to absorb 730 nm excitation energy. Meanwhile, due to the very weak absorption of NPTAT at 808 nm, the emission at 1060 nm of DCNPs under 808 nm excitation remained constant, which could serve as a stable reference signal for NIR-II biosensing. The NIR-II signal recovered under 730 nm excitation with NPTAT labeled bovine serum albumin (BSA) model drug release, achieving real-time monitoring of gastrointestinal drug release (Fig. 13C). Furthermore, using the microenvironment responsive molecular dye as an absorbing competitor could realize disease detection. Peng and coworkers developed ACIE nanohybrids containing DCNPs and NIR dye, compound 1, for the detection of H_2S in a liver failure mouse model (Fig. 13D). In the presence of H_2S, the emission at 1064 nm of DCNPs recovered along with compound 1 (competitive absorption of 808 nm excitation) destruction for NIR-II imaging of LPS induced hepatic inflammation.[101]

In this ACIE strategy, the ratio of the sensing signal to reference signal has been further used to achieve semi-quantitative ratiometric NIR-II biosensing. Zhang and coworkers also reported ACIE nanohybrids containing Er^{3+}-doped DCNPs, and NIR dye Cy7.5 (as absorbing competition acceptor) for monitoring lymphatic inflammation (Fig. 13E).[84] Cy7.5 modified on the surface of DCNPs act as a photon filtration layer for absorbing 808 nm excitation energy, leading to quenching of emission at 1550 nm under 808 nm excitation. Robust emission at 1550 nm under 980 nm excitation serves as a reference signal. Thus, NIR-II biosensing of the inflamed lymphatic system was achieved due to the decomposition of Cy7.5 (Fig. 13F). Meanwhile, they also reported 3D-printed bioactive glass scaffolds as ACIE nanohybrids containing Er^{3+}-doped DCNPs and NIR dye IR-808 (as absorbing competition acceptor) for monitoring the early inflammation, angiogenesis, and implant degradation during mouse skull repair (Fig. 13G).[65] ClO^- responsive IR-808 acted as

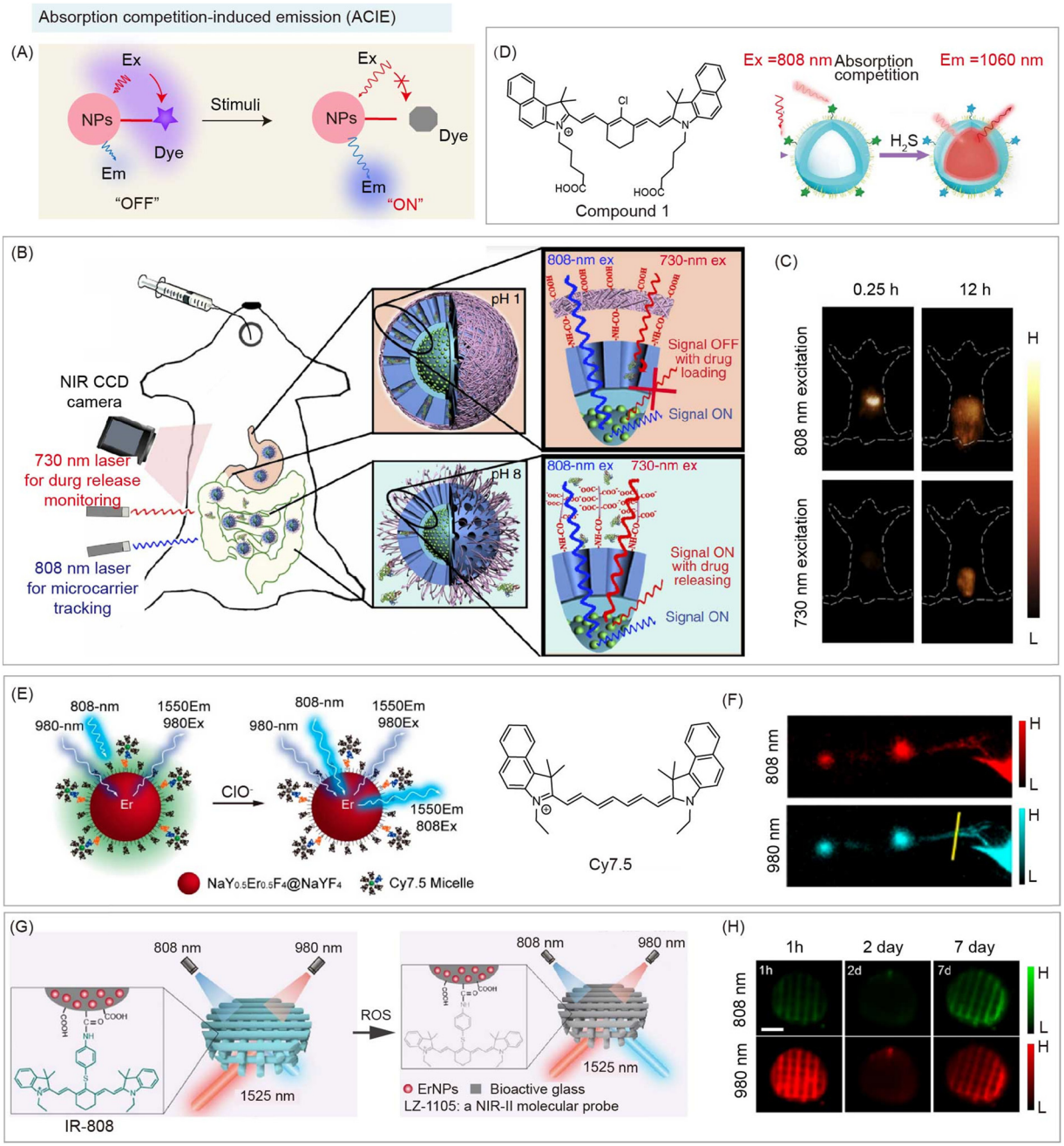

Fig. 13 ACIE based NIR-II organic/inorganic nanohybrids for biosensing. (A) Schematic of the absorption competition-induced emission (ACIE) system based nanohybrids before and after stimulation for NIR-II bio-sensing. (B) Schematic of ACIE nanohybrids containing DCNPs and NIR dye NPTAT (as the absorbing competition acceptor) for monitoring gastrointestinal drug release. (C) NIR-II imaging of mice at different times after oral nanohybrid administration. Reproduced with permission from ref. 66, copyright 2017, Springer. (D) Schematic of ACIE nanohybrids containing DCNPs and NIR dye Cy7.5 derivate for detection of H_2S (left). NIR-II imaging of LPS induced hepatic inflammation after nanohybrid administration (right). Reproduced with permission from ref. 101, copyright 2021, American Chemical Society. (E) Schematic of ACIE nanohybrids containing Er^{3+}-doped DCNPs and NIR dye Cy7.5 derivate (as the absorbing competition acceptor) for monitoring lymphatic inflammation. (F) NIR-II bioimaging of the inflamed lymphatic system after nanohybrid administration. Reproduced with permission from ref. 84, copyright 2019, American Chemical Society. (G) Schematic of the 3D-printed bioactive glass scaffold-based ACIE nanohybrids containing Er^{3+}-doped DCNPs and NIR dye IR-808 (as the absorbing competition acceptor) for monitoring of the early inflammation, angiogenesis, and implant degradation during mouse skull repair. (H) NIR-II bioimaging of the early inflammatory process during mouse skull repair after nanohybrid administration. Reproduced with permission from ref. 65, copyright 2022, American Chemical Society.

an absorbing competitor for 808 nm excitation. Thus, an early inflammatory process during mouse skull repair was observed after nanohybrid administration under 808 and 980 nm excitation (Fig. 13H).

The ACIE strategy fully uses the different absorbing abilities between organic dyes and inorganic nanoparticles. Without an energy transfer process, responsive nanohybrids could be constructed for biosensing. Compared to the secondary absorbance

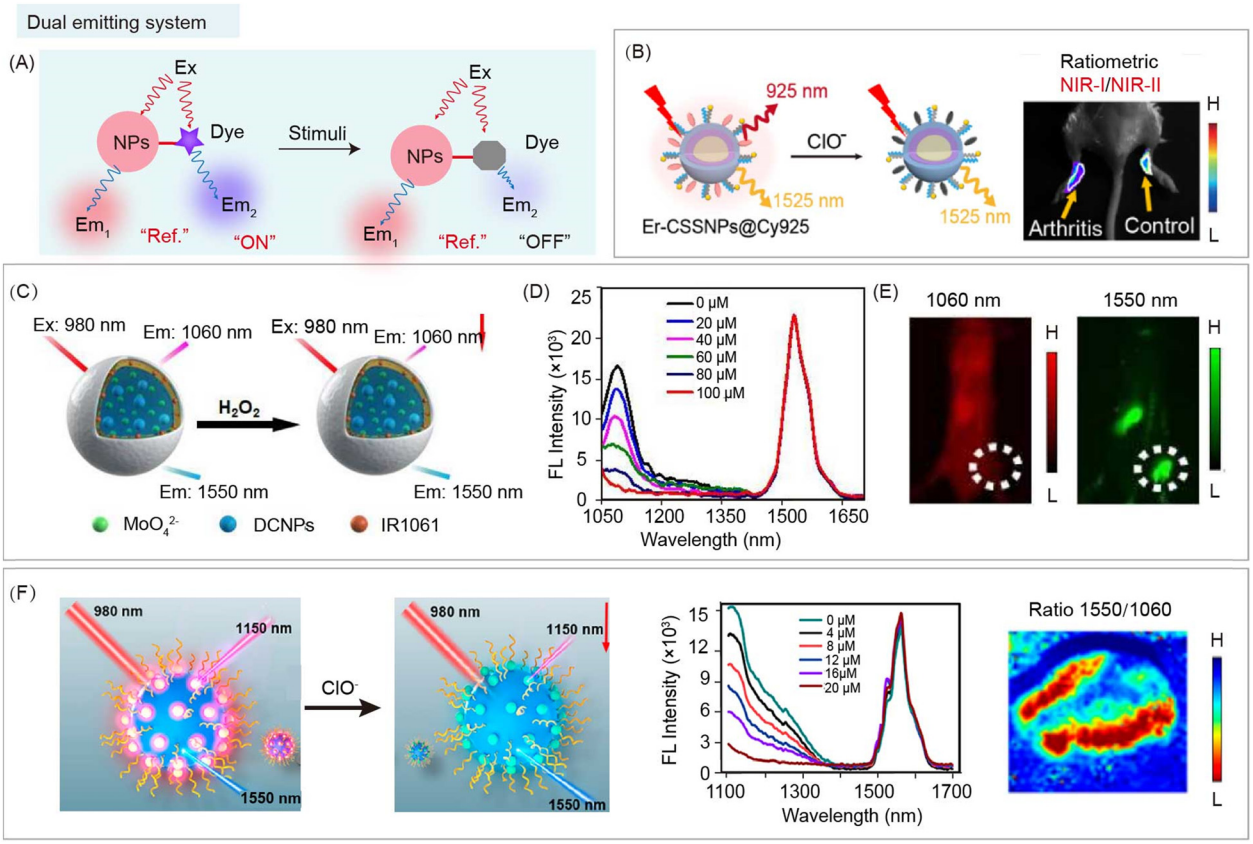

Fig. 14 Dual emitting organic/inorganic nanohybrids for NIR-II ratiometric biosensing. (A) Schematic of ratiometric nanohybrids before and after stimulation for NIR-II bio-sensing. (B) Schematic of nanohybrids Er-CSSNPs@Cy925 containing DCNPs (reference signals at 1525 nm) and NIR-I dye Cy925 (response signals at 925 nm) for ClO^- detection (left). Ratiometric NIR-I/NIR-II imaging of carrageenan induced arthritis mice after nanohybrid administration (right). Reproduced with permission from ref. 102, copyright 2019, American Chemical Society. (C) Schematic of CMTNs@IR1061/DCNPs nanohybrids containing MoO_4^{2-}, sodium carbonate, PEGylated liposomes, DCNPs (reference signals at 1550 nm), and NIR-II dye IR1061 (response signals at 1060 nm) for ratiometric measurement of H_2O_2. (D) H_2O_2 response of emission spectra of nanohybrids. (E) NIR-II imaging of MCF-7 tumor-bearing mice after nanohybrid administration. Reproduced with permission from ref. 103, copyright 2021, Wiley-VCH. (F) Schematic of DCNP@SeTT nanohybrids containing DCNPs (reference signals at 1550 nm) and NIR-I dye SeTT (response signals at 1150 nm) for ratiometric measurement of ClO^- (left). ClO^- responsive emission spectra of nanohybrids (middle). Ratiometric imaging of 4T1 tumor-bearing mice after nanohybrid administration (right). Reproduced with permission from ref. 104, copyright 2020, American Chemical Society.

strategy in which organic component requires absorbance in the NIR-II region to quench the emitter, the ACIE strategy has more choices in organic components because the organic molecule only needs to absorb excitation lasers, most of which are in visible and NIR-I region. Furthermore, the longer emission wavelength of nanohybrids could be used for biosensing, such as collection window beyond 1500 nm, which could be hardly realized by the secondary absorbance strategy.

4.5 Dual emitting system based nanohybrids

Besides the above-mentioned FRET, dye sensitizing, secondary absorbance, and ACIE, both organic and inorganic materials can serve as emitters in different channels. Through ratiometric imaging between the responsive organic sensing signal and robust inorganic reference signal, NIR-II biosensing could be realized by the nanohybrids (Fig. 14A). Li and co-workers reported 808 nm excited nanohybrids Er-CSSNPs@Cy925 containing Er^{3+} doped DCNPs (as the reference signal at 1525 nm) and NIR-I dye Cy925 (as the responsive signal at 925 nm) for ClO^- detection in living arthritis mice (Fig. 14B).[102] After reacting with ClO^- at the arthritis site, fluorescence emission at 925 nm decreased along with the decomposition of Cy925, while the emission at 1525 nm remained unchanged. Thus, the ratio of two NIR emission channels (NIR-I/NIR-II) can be used for bio-sensing of arthritis. Similarly, Chen and co-workers developed CMTNs@IR1061/DCNPs nanohybrids containing DCNPs (reference signal at 1550 nm) and NIR-II dye IR1061 (response signal at 1060 nm) for ratiometric measurement of $^1O_2$ generation (Fig. 14C).[103] In the presence of H_2O_2, $^1O_2$ was generated under CMTNs catalysis, causing a gradual decrease of fluorescence emission at 1060 nm along with the decomposition of IR1061, while the emission at 1550 nm remained unchanged (Fig. 14D). Dual NIR-II emissive nanohybrids can be used for monitoring H_2O_2 in MCF-7 tumor-bearing mice (Fig. 14E). Meanwhile, Song and co-workers reported DCNP@SeTT nanohybrids containing DCNPs (reference signal at 1550 nm) and NIR-I dye SeTT (response signal at 1150 nm) for ratiometric measurement of ClO^- (Fig. 14F).[104] After reacting

with ClO^- at the osteoarthritis site, fluorescence emission at 1150 nm gradually decreased along with decomposition of SeTT through oxidation by ClO^-, while the emission at 1550 nm remained unchanged. Thus, the ratio of two NIR-II emission signals can be used for ClO^- bio-sensing in a rabbit model of osteoarthritis. In these dual emitting nanohybrids, organic and inorganic components do not interfere with each other, and there is no interaction between them. Hence, it is easy to design and obtain these nanohybrids for semi-quantitative biosensing.

4.6 NIR-II lifetime imaging

When penetrating the bio-tissue, a variety of interactions would occur between biological tissues and excitation/emission photons, including interface reflection for excitation light and tissue scattering of excitation/emission light, leading to the unavoidable tissue autofluorescence and signal intensity attenuation.[4,8,78,88] Therefore, it is difficult to achieve *in vivo* quantitative analysis using fluorescence (or luminescence) intensity based bioimaging, even in the NIR-II region. Ratiometric fluorescence imaging can eliminate the interference of probe concentration. However, the different photon absorbance and scattering at different emission wavelengths still hamper the accuracy of ratiometric fluorescence based quantitative biosensing.[8] Meanwhile, excitation-free optical imaging, including bioluminescence imaging, and afterglow imaging, can eliminate real-time excitation to minimize background noise.[105–107] Unfortunately, photons emitted from materials still interact with biological tissue and affect quantification.

Fluorescence (or luminescence) lifetime is related to the time that photons stay on average in the excited state of fluorophore before emission takes place. It is an essential feature of a fluorophore, which is independent of the excitation and emission wavelength range and emission intensity.[88] Therefore, compared with fluorescence (or luminescence) intensity imaging, lifetime imaging is a promising method for bioimaging and biosensing.[78] Lifetime-based imaging has great potential for distinguishing and locating different probes with

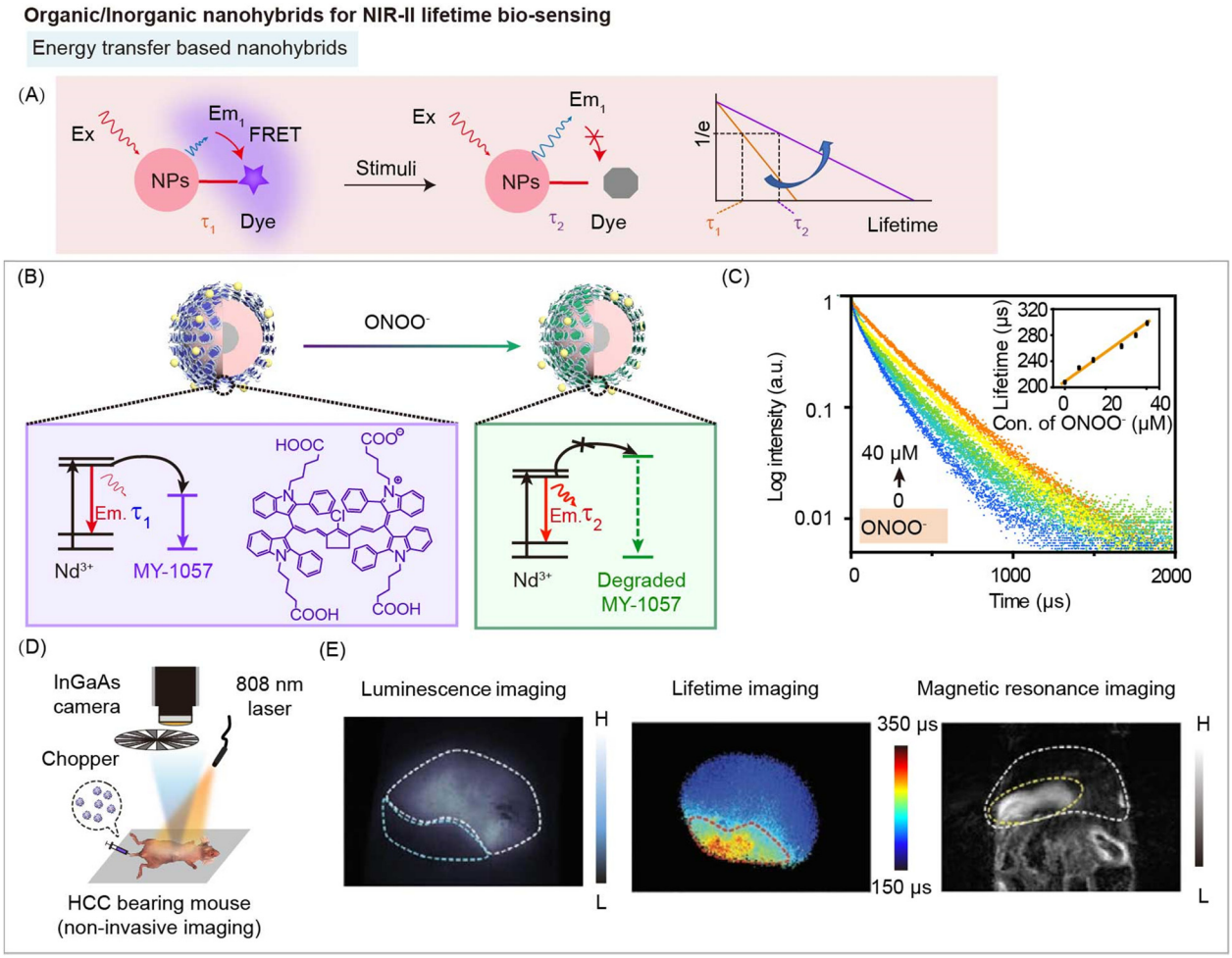

Fig. 15 Organic/inorganic nanohybrids for NIR-II lifetime bio-sensing. (A) Schematic of energy transfer induced NIR-II luminescence lifetime variation before and after stimulation for bio-sensing. (B) Schematic of FRET nanohybrids DSNP@MY-1057-GPC-3 containing DCNPs (as donor) and NIR-II dye MY-1057 (as the acceptor) for hepatocellular carcinoma (HCC) detection and $ONOO^-$ quantify. (C) Luminescence lifetime decay profile of nanohybrids in response to $ONOO^-$. (D) Experimental setup used for NIR-II luminescence lifetime imaging. (E) NIR-II intensity imaging (left), lifetime imaging (middle) and magnetic resonance imaging (MRI) (right) of HCC tumor bearing mouse after nanohybrid administration. Reproduced with permission from ref. 49, copyright 2020, Wiley-VCH.

different lifetimes at the same excitation and emission wavelengths. For example, Nothdurft and coworkers have reported a fluorescence intensity and lifetime imaging system, which can observe intracellular distributions of two dyes, cypate and 3,3-diethylthiatricarbocyanine iodine (DTTCI), with similar emission wavelengths (between 800 and 840 nm) under 773 nm laser excitation.[108] Intensity-based imaging failed to distinguish distribution of co-incubated two dyes due to the similar emission wavelength. However, as for lifetime-based imaging, there are distinct differences to distinguish and locate the distribution of the two dyes because of the different lifetime values of 0.5 and 1.1 ns. Meanwhile, Ortgies and coworkers developed a series of Yb^{3+}-doped RENPs with different lifetimes (0.1–1.5 ms) under 800 nm laser excitation.[109] Lifetime-based imaging can observe the distribution of $NaY_{0.7}Yb_{0.1}Nd_{0.2}F_4$@$CaF_2$ NPs and $NaY_{0.6}Yb_{0.1}Nd_{0.3}F_4$@$CaF_2$ NPs with different lifetime values of 0.7 and 1.3 ms after oral and intravenous administration in the same emission wavelength. Thus, compared with intensity-based imaging, lifetime-based imaging overcomes spectral overlap, tissue background interference, excitation and emission wavelength and intensity, which is a promising method for quantitative biosensing.

The energy transfer between organic and inorganic components can change the fluorescence (or luminescence) lifetime of the energy donor in nanohybrids, which could be used for lifetime bio-sensing (Fig. 15A). Other processes in the nanohybrids, such as secondary absorption, and ACIE, will not affect the lifetime of nanohybrids, so they cannot be used for lifetime biosensing. Zhang and coworkers have developed energy transfer nanohybrids DSNP@MY-1057-GPC-3 containing Nd^{3+}-doped DCNPs (donor) and NIR-II dye MY-1057 (acceptor) for hepatocellular carcinoma (HCC) detection and quantitative $ONOO^-$ sensing (Fig. 15B).[49] After reacting with $ONOO^-$, a kind of RNS in the tumor, luminescence lifetime of nanohybrids gradually recovered from 203 μs to 298 μs along with decomposition of MY-1057 (Fig. 15C). Compared with fluorescence intensity imaging, lifetime imaging of nanohybrids showed negligible change under different tissue penetration depths, indicating that lifetime imaging has high accuracy for quantitative detection. NIR-II luminescence lifetime imaging and intensity imaging can be achieved using an InGaAs camera (Fig. 15D). HCC lesions can be easily distinguished from normal tissue by NIR-II luminescence lifetime imaging, but hardly by luminescence intensity imaging. Meanwhile, luminescence lifetime imaging, magnetic resonance imaging (MRI), and dissected imaging of the HCC tumor bearing liver were consistent, suggesting the accuracy of lifetime imaging (Fig. 15E).

Luminescence lifetime imaging is an important modality to detect and image analytes or physiological and pathological processes because of its independence of sensor concentration or initial signal intensity. Combined with the advantages of deep tissue penetration, NIR-II luminescence lifetime imaging provides more opportunities for qualitative and quantitative bio-sensing in deep biological tissues.

5. Conclusion and outlook

In this tutorial review, we summarized the reported NIR-II organic/inorganic nanohybrids, including the types of organic

Table 1 Summary of NIR-II organic/inorganic nanohybrids

	Organic species	Inorganic species	Designed mechanism	Biomedical applications	Ref.
NIR-II bio-imaging	Azobenzene/β-cyclodextrins	Tm^{3+}-UCNPs/Nd^{3+}-DCNPs	*In vivo* assembly/disassembly	Peritoneal metastases tumor imaging	19
	DNA	Nd^{3+}-DCNPs	*In vivo* assembly	Imaging guided ovarian tumor resection	83
	IR-140	HMSNs	J-Aggregates	Metabolic imaging	82
	FD-1080	MSTPs	J-Aggregates	Imaging guided osteosynthesis	81
	ICG	DCNPs	Dye sensitizing	*In situ* imaging	62
	Alk-pi	Er^{3+}-UCNPs	Dye sensitizing	Vascular imaging	63
NIR-II bio-sensing	GSH	Nd^{3+}-DCNPs	*In vivo* assembly	Inflammation biosensing	25
	Fmoc-His, DOX, A1094	Ag_2S	*In vivo* disassembly	Peritoneal metastasis tumor biosensing	85
	PolyRu, IR1061	Gold nanorod	*In vivo* disassembly	Imaging guided cancer synergistic therapy	92
	A1094	Ag_2S	$ONOO^-$ responsive FRET system	Traumatic brain injury bio-sensing	50
	FD-1080	Nd^{3+}-DCNPs	ClO^- responsive FRET system	Analysis of real milk samples	96
	FD-1080 J-aggregates	Nd^{3+}/Er^{3+}-DCNPs	ClO^- responsive FRET system	Inflammation biosensing	97
	NPh	Nd^{3+}/Er^{3+}-DCNPs	GSH responsive dye sensitizing	Orthotopic colon cancer biosensing	64
	IR1061	Er^{3+}-UCNPs	H_2O_2 responsive secondary absorption system	Inflammation dynamic detection	95
	Cy7.5 derivate	Nd^{3+}-DCNPs	H_2S responsive ACIE system	Hepatic inflammation biosensing	101
	NPTAT, BSA, SSPI	Nd^{3+}-DCNPs	pH responsive ACIE system	Monitoring gastrointestinal drug release	66
	Cy7.5 derivate	Er^{3+}-UCNPs	ClO^- responsive ACIE system	Inflammation detection	84
	IR-808	Er^{3+}-UCNP	ClO^- responsive ACIE system	*In situ* bone repair	65
	Cy925	Er^{3+}-DCNPs	ClO^- responsive dual emitting system	Arthritis bio-sensing	102
	IR1061	Er^{3+}-DCNPs, MoO_4^{2-}	$^1O_2$ responsive dual emitting system	Monitoring tumor H_2O_2	103
	SeTT	Er^{3+}-DCNPs	ClO^- responsive dual emitting system	Osteoarthritis bio-sensing	104
NIR-II lifetime imaging	MY-1057	Nd^{3+}-DCNPs	$ONOO^-$-activatable FRET system	Imaging of hepatocellular carcinoma	49

and inorganic species, advantages, and biomedical applications (Table 1). Organic and inorganic species can be divided into two categories: materials with NIR-II optical properties, and functional materials without optical properties. Polymethine dyes (FD-1080, LZ-1105, MY-1057, IR1061), D–A–D dyes (SeTT), and functional moieties (DNA, responsive ligands), are used as organic species. RENPs (Tm^{3+}-UCNPs, Nd^{3+}-DCNPs), QDs (Ag_2S), and mesoporous silica are employed as inorganic species. Organic/inorganic nanohybrids can integrate the advantages including responsiveness of organic species and stable fluorescence (or luminescence) properties of inorganic species to obtain new optical properties, chemical characteristics, and biological properties, providing unique performance. For instance, nanohybrids with self-aggregation or disaggregation features can not only specifically accumulate in lesions, but also reduce the nanomaterial capture in normal tissues, thereby improving imaging SNR. Meanwhile, by combining their optical properties, some strategies, including FRET, dye sensitizing methods, secondary absorption, ACIE, and dual emitting system are constructed for biomedical applications, such as bioimaging of brain vasculature, monitoring drug release, and biosensing of traumatic brain injury. Besides, energy transfer based NIR-II nanohybrids can also serve as luminescence lifetime probes for quantitative biosensing in deep biological tissues.

Although promising, NIR-II organic/inorganic nanohybrids for biomedical applications still face many challenges. From the design of nanohybrids to their biomedical applications, the following issues should be considered: (1) Developing more NIR-II organic/inorganic nanohybrids with new materials. Currently, only a few organic and inorganic materials have been used to construct NIR-II nanohybrids, including RENPs, QDs, and polymethine dyes. In the future, other materials such as semiconducting polymer nanomaterials, functional small molecules, and metal clusters, may also be employed. Each class of materials has its unique properties, such as metal clusters with magnetic properties. Through full integration of the characteristics of organic and inorganic species, nanohybrids will have more unique properties for biomedical applications. (2) Developing NIR-II organic/inorganic nanohybrids with excitation and emission in NIR-IIa and NIR-IIb regions. At present, the fluorescence emission wavelengths of most NIR-II organic/inorganic nanohybrids are concentrated in the range of 1000–1200 nm, mainly due to the difficult design and synthesis of molecular dyes with spectral wavelengths beyond 1200 nm. In fact, NIR-IIa and NIR-IIb regions should be further valued for biomedical applications, especially the NIR-IIb region, owing to the extremely low tissue absorption, scattering, and autofluorescence at a longer wavelength. Besides, the excitation wavelength of nanohybrids is also a concern. The excitation wavelengths of reported nanohybrids are mainly located in the NIR-I region. As mentioned above, photons in the NIR-II region have deeper tissue penetration and higher maximum safe exposure, compared with visible and NIR-I photons. Thus, developing nanohybrids with excitation and emission in the NIR-II region is a promising direction for biomedical applications. (3) Developing NIR-II organic/inorganic nanohybrids with multiplexed activation. Diseases are accompanied by the changes of multiple physiological parameters in biological tissues, for example, low pH value, high GSH, H_2O_2, and enzymes.[110] The currently reported NIR-II nanohybrids are mostly responsive to a single disease related stimuli for bio-sensing. However, in a complex and dynamic physiological environment, this method may suffer from non-specific responses and cause false positive results. (4) Developing theranostic potential of NIR-II organic/inorganic nanohybrids. The currently reported NIR-II nanohybrids mainly focus on bioimaging and biosensing of analytes. Integrating the therapeutic potential of organic and inorganic species, NIR-II organic/inorganic nanohybrids can realize the diagnosis and treatment of diseases simultaneously. Thus, nanohybrids have great potential application prospects in the field of theranostics. (5) Developing more NIR-II organic/inorganic nanohybrids for fluorescence (or luminescence) lifetime imaging. Compared with fluorescence (or luminescence) intensity imaging, fluorescence (or luminescence) lifetime imaging has some further advantages, including independence of probe concentration and unknown tissue penetration depth. Meanwhile, fluorescence (or luminescence) lifetime imaging provides a powerful imaging modality with quantitative analysis ability in biomedical applications. Thus, researchers should pay more attention to biomedical applications of organic/inorganic nanohybrids using fluorescence (or luminescence) lifetime imaging. (6) The large absorption cross-section and high extinction coefficient of organic dyes make them superior contrast agents for photoacoustic imaging, and responsive organic molecules could further lead to photoacoustic signal changing. Thus, like fluorescence and luminescence imaging and sensing, the NIR-II photoacoustic technique may be combined with the organic/inorganic nanohybrids to realize biomedical imaging and sensing under deep tissue.

Conflicts of interest

There are no conflicts to declare.

Acknowledgements

The work is financially supported by the National Key R&D Program of China (2020YFA0908800, 2018YFA0704000), the Basic Research Program of Shenzhen (JCYJ20180305163323140, JCYJ20200109105620482, JCYJ20180507182413022), the Shenzhen Science and Technology Program (KQTD20190929172538530), the National University of Singapore Startup Fund (NUHSRO/2020/133/Startup/08), the NUS School of Medicine Nanomedicine Translational Research Programme (NUHSRO/2021/034/TRP/09/Nanomedicine), and the National Medical Research Council (NMRC) Centre Grant Programme (CG21APR1005).

References

1 V. Ntziachristos, J. Ripoll, L. V. Wang and R. Weissleder, *Nat. Biotechnol.*, 2005, **23**, 313–320.

2 B. H. Li, Y. L. Zhang, F. S. Li, W. Wang, J. Liu, M. Liu, Y. Cui, X. B. Li and B. L. Li, *Sens. Actuators, B*, 2016, **233**, 479–485.
3 W. Sun, S. Guo, C. Hu, J. Fan and X. Peng, *Chem. Rev.*, 2016, **116**, 7768–7817.
4 G. Hong, A. L. Antaris and H. Dai, *Nat. Biomed. Eng.*, 2017, **1**, 0010.
5 J. Li and K. Pu, *Chem. Soc. Rev.*, 2019, **48**, 38–71.
6 Y. Sun, F. Ding, Z. Chen, R. Zhang, C. Li, Y. Xu, Y. Zhang, R. Ni, X. Li, G. Yang, Y. Sun and P. J. Stang, *Proc. Natl. Acad. Sci. U. S. A.*, 2019, **116**, 16729–16735.
7 S. Wang, B. Li and F. Zhang, *ACS Cent. Sci.*, 2020, **6**, 1302–1316.
8 M. Zhao, B. Li, H. Zhang and F. Zhang, *Chem. Sci.*, 2021, **12**, 3448–3459.
9 Y. Sun, F. Ding, Z. Zhou, C. Li, M. Pu, Y. Xu, Y. Zhan, X. Lu, H. Li, G. Yang, Y. Sun and P. J. Stang, *Proc. Natl. Acad. Sci. U. S. A.*, 2019, **116**, 1968–1973.
10 Z. Feng, T. Tang, T. Wu, X. Yu, Y. Zhang, M. Wang, J. Zheng, Y. Ying, S. Chen, J. Zhou, X. Fan, D. Zhang, S. Li, M. Zhang and J. Qian, *Light: Sci. Appl.*, 2021, **10**, 197.
11 L. Shi, L. A. Sordillo, A. Rodriguez-Contreras and R. Alfano, *J. Biophotonics*, 2016, **9**, 38–43.
12 R. H. Wilson, K. P. Nadeau, F. B. Jaworski, B. J. Tromberg and A. J. Durkin, *J. Biomed. Opt.*, 2015, **20**, 030901.
13 B. Li, L. Lu, M. Zhao, Z. Lei and F. Zhang, *Angew. Chem., Int. Ed.*, 2018, **57**, 7483–7487.
14 Y. Tsukasaki, A. Komatsuzaki, Y. Mori, Q. Ma, Y. Yoshioka and T. Jin, *Chem. Commun.*, 2014, **50**, 14356–14359.
15 K. Suhling, L. M. Hirvonen, J. A. Levitt, P.-H. Chung, C. Tregidgo, A. Le Marois, D. A. Rusakov, K. Zheng, S. Ameer-Beg, S. Poland, S. Coelho, R. Henderson and N. Krstajic, *Med. Photonics*, 2015, **27**, 3–40.
16 B. Del Rosal, D. H. Ortgies, N. Fernandez, F. Sanz-Rodriguez, D. Jaque and E. M. Rodriguez, *Adv. Mater.*, 2016, **28**, 10188–10193.
17 A. Almutairi, S. J. Guillaudeu, M. Y. Berezin, S. Achilefu and J. M. Frechet, *J. Am. Chem. Soc.*, 2008, **130**, 444–445.
18 Y. Liu, Y. Gu, W. Yuan, X. Zhou, X. Qiu, M. Kong, Q. Wang, W. Feng and F. Li, *Adv. Sci.*, 2020, **7**, 1902929.
19 M. Zhao, B. Li, P. Wang, L. Lu, Z. Zhang, L. Liu, S. Wang, D. Li, R. Wang and F. Zhang, *Adv. Mater.*, 2018, **30**, 1804982.
20 A. P. Alivisatos, *Science*, 1996, **271**, 933–937.
21 Y. Sun, M. Ding, X. Zeng, Y. Xiao, H. Wu, H. Zhou, B. Ding, C. Qu, W. Hou, A. G. A. Er-bu, Y. Zhang, Z. Cheng and X. Hong, *Chem. Sci.*, 2017, **8**, 3489–3493.
22 B. Li, M. Zhao, L. Feng, C. Dou, S. Ding, G. Zhou, L. Lu, H. Zhang, F. Chen, X. Li, G. Li, S. Zhao, C. Jiang, Y. Wang, D. Zhao, Y. Cheng and F. Zhang, *Nat. Commun.*, 2020, **11**, 3102.
23 T. Wang, S. Wang, Z. Liu, Z. He, P. Yu, M. Zhao, H. Zhang, L. Lu, Z. Wang, Z. Wang, W. Zhang, Y. Fan, C. Sun, D. Zhao, W. Liu, J. G. Bunzli and F. Zhang, *Nat. Mater.*, 2021, **20**, 1571–1578.
24 K. Welsher, Z. Liu, S. P. Sherlock, J. T. Robinson, Z. Chen, D. Daranciang and H. Dai, *Nat. Nanotechnol.*, 2009, **4**, 773–780.
25 M. Zhao, R. Wang, B. Li, Y. Fan, Y. Wu, X. Zhu and F. Zhang, *Angew. Chem., Int. Ed.*, 2019, **58**, 2050–2054.
26 B. Li, M. Zhao and F. Zhang, *ACS Mater. Lett.*, 2020, **2**, 905–917.
27 Z. Lei and F. Zhang, *Angew. Chem., Int. Ed.*, 2021, **60**, 16294–16308.
28 J. A. Carr, D. Franke, J. R. Caram, C. F. Perkinson, M. Saif, M. G. Bawendi, O. T. Bruns, V. Askoxylakis, M. Datta, D. Fukumura, R. K. Jain and M. Datta, *Proc. Natl. Acad. Sci. U. S. A.*, 2018, **115**, 4465–4470.
29 S. Zhu, Z. Hu, R. Tian, B. C. Yung, Q. Yang, S. Zhao, D. O. Kiesewetter, G. Niu, H. Sun, A. L. Antaris and X. Chen, *Adv. Mater.*, 2018, **30**, 1802546.
30 R. Tian, S. Zhu, J. Lau, S. Chandra, G. Niu, D. O. Kiesewetter, X. Chen, Q. Zeng, B. R. Brooks, R. Ertsey, K. S. Hettie, T. Teraphongphom, Z. Hu, H. Sun, X. Zhang, A. L. Antaris, B. R. Brooks and X. Chen, *Sci. Adv.*, 2019, **5**, eaaw067.
31 A. L. Antaris, H. Chen, Y. Sun, C. Qu, Z. Deng, X. Hu, X. Hong, A. L. Antaris, G. Hong, S. Diao, B. Zhang, X. Zhang, O. K. Yaghi, Z. R. Alamparambil, H. Dai, H. Chen, K. Cheng and Z. Cheng, *Nat. Mater.*, 2016, **15**, 235–242.
32 Y. Sun, C. Qu, H. Chen, M. He, C. Tang, K. Shou, S. Hong, M. Yang, Y. Jiang, B. Ding, Y. Xiao, L. Xing, X. Hong and Z. Cheng, *Chem. Sci.*, 2016, **7**, 6203–6207.
33 A. L. Antaris, H. Chen, S. Diao, Z. Ma, Z. Zhang, S. Zhu, J. Wang, A. X. Lozano, Q. Fan, L. Chew, M. Zhu, K. Cheng, X. Hong, H. Dai and Z. Cheng, *Nat. Commun.*, 2017, **8**, 15269.
34 Q. Yang, Z. Ma, H. Wang, B. Zhou, S. Zhu, Y. Zhong, J. Wang, H. Wan, A. Antaris, R. Ma, X. Zhang, J. Yang, X. Zhang, H. Sun, W. Liu, Y. Liang and H. Dai, *Adv. Mater.*, 2017, **29**, 1605497.
35 H. Ma, C. Liu, Z. Hu, P. Yu, X. Zhu, R. Ma, Z. Sun, C.-H. Zhang, H. Sun, S. Zhu and Y. Liang, *Chem. Mater.*, 2020, **32**, 2061–2069.
36 Q. Yang, Z. Hu, S. Zhu, R. Ma, H. Ma, Z. Ma, H. Wan, T. Zhu, Z. Jiang, W. Liu, L. Jiao, H. Sun, Y. Liang and H. Dai, *J. Am. Chem. Soc.*, 2018, **140**, 1715–1724.
37 X. Zeng, Y. Xiao, J. Lin, S. Li, H. Zhou, J. Nong, G. Xu, H. Wang, F. Xu, J. Wu, Z. Deng and X. Hong, *Adv. Healthcare Mater.*, 2018, **7**, 1800589.
38 J. Lin, X. Zeng, Y. Xiao, L. Tang, J. Nong, Y. Liu, H. Zhou, B. Ding, F. Xu, H. Tong, Z. Deng and X. Hong, *Chem. Sci.*, 2019, **10**, 1219–1226.
39 Y. Sun, X. Zeng, Y. Xiao, C. Liu, H. Zhu, H. Zhou, Z. Chen, F. Xu, J. Wang, M. Zhu, J. Wu, M. Tian, H. Zhang, Z. Deng, Z. Cheng and X. Hong, *Chem. Sci.*, 2018, **9**, 2092–2097.
40 H. Wan, J. Yue, S. Zhu, T. Uno, X. Zhang, Q. Yang, K. Yu, G. Hong, J. Wang, L. Li, Z. Ma, H. Gao, Y. Zhong, J. Su, A. L. Antaris, Y. Xia, J. Luo, Y. Liang and H. Dai, *Nat. Commun.*, 2018, **9**, 1171.
41 Y. Fang, J. Shang, D. Liu, W. Shi, X. Li and H. Ma, *J. Am. Chem. Soc.*, 2020, **142**, 15271–15275.
42 M. Zhao, J. Wang, Z. Lei, L. Lu, S. Wang, H. Zhang, B. Li and F. Zhang, *Angew. Chem., Int. Ed.*, 2021, **60**, 5091–5095.

43 L. Bai, P. Sun, Y. Liu, H. Zhang, W. Hu, W. Zhang, Z. Liu, Q. Fan, L. Li and W. Huang, *Chem. Commun.*, 2019, **55**, 10920–10923.
44 K. Dou, W. Feng, C. Fan, Y. Cao, Y. Xiang and Z. Liu, *Anal. Chem.*, 2021, **93**, 4006–4014.
45 G. Xu, Q. Yan, X. Lv, Y. Zhu, K. Xin, B. Shi, R. Wang, J. Chen, W. Gao, P. Shi, C. Fan, C. Zhao and H. Tian, *Angew. Chem., Int. Ed.*, 2018, **57**, 3626–3630.
46 J. Zou, L. Li, J. Zhu, X. Li, Z. Yang, W. Huang and X. Chen, *Adv. Mater.*, 2021, **33**, 2103627.
47 C. S. L. Rathnamalala, J. N. Gayton, A. L. Dorris, S. A. Autry, W. Meador, N. I. Hammer, J. H. Delcamp and C. N. Scott, *J. Org. Chem.*, 2019, **84**, 13186–13193.
48 Q. Zhang, P. Yu, Y. Fan, C. Sun, H. He, X. Liu, L. Lu, M. Zhao, H. Zhang and F. Zhang, *Angew. Chem., Int. Ed.*, 2021, **60**, 3967–3973.
49 M. Zhao, B. Li, Y. Wu, H. He, X. Zhu, H. Zhang, C. Dou, L. Feng, Y. Fan and F. Zhang, *Adv. Mater.*, 2020, **32**, 2001172.
50 C. Li, W. Li, H. Liu, Y. Zhang, G. Chen, Z. Li and Q. Wang, *Angew. Chem., Int. Ed.*, 2020, **59**, 247–252.
51 B. Li, H. Liu, Y. He, M. Zhao, C. Ge, M. R. Younis, P. Huang, X. Chen and J. Lin, *Angew. Chem., Int. Ed.*, 2022, **61**, e202200025.
52 M. Y. Lucero, A. K. East, C. J. Reinhardt, A. C. Sedgwick, S. Su, M. C. Lee and J. Chan, *J. Am. Chem. Soc.*, 2021, **143**, 7196–7202.
53 E. D. Cosco, J. R. Caram, O. T. Bruns, D. Franke, R. A. Day, E. P. Farr, M. G. Bawendi and E. M. Sletten, *Angew. Chem., Int. Ed.*, 2017, **56**, 13126–13129.
54 B. Ding, Y. Xiao, H. Zhou, X. Zhang, C. Qu, F. Xu, Z. Deng, Z. Cheng and X. Hong, *J. Med. Chem.*, 2018, **62**, 2049–2059.
55 Z. Lei, C. Sun, P. Pei, S. Wang, D. Li, X. Zhang and F. Zhang, *Angew. Chem., Int. Ed.*, 2019, **58**, 8166–8171.
56 S. Wang, Y. Fan, D. Li, C. Sun, Z. Lei, L. Lu, T. Wang and F. Zhang, *Nat. Commun.*, 2019, **10**, 1058.
57 Y. Shi, W. Yuan, Q. Liu, M. Kong, Z. Li, W. Feng, K. Hu and F. Li, *ACS Mater. Lett.*, 2019, **1**, 418–424.
58 D. Liu, Z. He, Y. Zhao, Y. Yang, W. Shi, X. Li and H. Ma, *J. Am. Chem. Soc.*, 2021, **143**, 17136–17143.
59 Z. Qin, T. B. Ren, H. Zhou, X. Zhang, L. He, Z. Li, X. B. Zhang and L. Yuan, *Angew. Chem., Int. Ed.*, 2022, **61**, e202201541.
60 M.-H. Liu, Z. Zhang, Y.-C. Yang and Y.-H. Chan, *Angew. Chem., Int. Ed.*, 2021, **60**, 983–989.
61 V. G. Bandi, M. P. Luciano, M. Saccomano, N. L. Patel, T. S. Bischof, J. G. P. Lingg, P. T. Tsrunchev, M. N. Nix, B. Ruehle, C. Sanders, L. Riffle, C. M. Robinson, S. Difilippantonio, J. D. Kalen, U. Resch-Genger, J. Ivanic, O. T. Bruns and M. J. Schnermann, *Nat. Methods*, 2022, **19**, 353–358.
62 W. Shao, G. Chen, A. N. Kuzmin, H. L. Kutscher, A. Pliss, T. Y. Ohulchanskyy and P. N. Prasad, *J. Am. Chem. Soc.*, 2016, **138**, 16192–16195.
63 Q. Wang, T. Liang, J. Wu, Z. Li and Z. Liu, *ACS Appl. Mater. Interfaces*, 2021, **13**, 29303–29312.
64 C. Wang, H. Lin, X. Ge, J. Mu, L. Su, X. Zhang, M. Niu, H. Yang and J. Song, *Adv. Funct. Mater.*, 2021, **31**, 2009942.
65 P. Pei, H. Hu, Y. Chen, S. Wang, J. Chen, J. Ming, Y. Yang, C. Sun, S. Zhao and F. Zhang, *Nano Lett.*, 2022, **22**, 783–791.
66 R. Wang, L. Zhou, W. Wang, X. Li and F. Zhang, *Nat. Commun.*, 2017, **8**, 14702.
67 Y. Xu, B. Li, L. Xiao, J. Ouyang, S. Sun and Y. Pang, *Chem. Commun.*, 2014, **50**, 8677–8680.
68 M. Zhao, B. Li, Y. Fan and F. Zhang, *Adv. Healthcare Mater.*, 2019, **8**, 1801650.
69 J. Wen, K. Yang, F. Liu, H. Li, Y. Xu and S. Sun, *Chem. Soc. Rev.*, 2017, **46**, 6024–6045.
70 C. Kim, G. Y. Tonga, B. Yan, C. S. Kim, S. T. Kim, M. H. Park, Z. Zhu, B. Duncan, B. Creran and V. M. Rotello, *Org. Biomol. Chem.*, 2015, **13**, 2474–2479.
71 A. Nano, A. L. Furst, M. G. Hill and J. K. Barton, *J. Am. Chem. Soc.*, 2021, **143**, 11631–11640.
72 M. Molina, M. Asadian-Birjand, J. Balach, J. Bergueiro, E. Miceli and M. Calderón, *Chem. Soc. Rev.*, 2015, **44**, 6161–6186.
73 R. Tong, L. Tang, L. Ma, C. Tu, R. Baumgartner and J. Cheng, *Chem. Soc. Rev.*, 2014, **43**, 6982–7012.
74 J. Zhou, W. Zhang, C. Hong and C. Pan, *ACS Appl. Mater. Interfaces*, 2015, **7**, 3618–3625.
75 O. T. Bruns, T. S. Bischof, D. K. Harris, D. Franke, Y. Shi, L. Riedemann, A. Bartelt, F. B. Jaworski, J. A. Carr and C. J. Rowlands, *Nat. Biomed. Eng.*, 2017, **1**, 56.
76 Y. Liu, Y. Li, S. Koo, Y. Sun, Y. Liu, X. Liu, Y. Pan, Z. Zhang, M. Du, S. Lu, X. Qiao, J. Gao, X. Wang, Z. Deng, X. Meng, Y. Xiao, J. S. Kim and X. Hong, *Chem. Rev.*, 2022, **122**, 209–268.
77 D. Naczynski, M. Tan, M. Zevon, B. Wall, J. Kohl, A. Kulesa, S. Chen, C. Roth, R. Riman and P. Moghe, *Nat. Commun.*, 2013, **4**, 1–10.
78 Y. Fan, P. Wang, Y. Lu, R. Wang, L. Zhou, X. Zheng, X. Li, J. A. Piper and F. Zhang, *Nat. Nanotechnol.*, 2018, **13**, 941–946.
79 Y. Zhang, G. Hong, Y. Zhang, G. Chen, F. Li, H. Dai and Q. Wang, *ACS Nano*, 2012, **6**, 3695–3702.
80 T. Zhao, L. Chen, R. Lin, P. Zhang, K. Lan, W. Zhang, X. Li and D. Zhao, *Acc. Mater. Res.*, 2020, **1**, 100–114.
81 C. Sun, X. Sun, P. Pei, H. He, J. Ming, X. Liu, M. Liu, Y. Zhang, Y. Xia, D. Zhao, X. Li, Y. Xie and F. Zhang, *Adv. Funct. Mater.*, 2021, **31**, 2100656.
82 W. Chen, C. A. Cheng, E. D. Cosco, S. Ramakrishnan, J. G. P. Lingg, O. T. Bruns, J. I. Zink and E. M. Sletten, *J. Am. Chem. Soc.*, 2019, **141**, 12475–12480.
83 P. Wang, Y. Fan, L. Lu, L. Liu, L. Fan, M. Zhao, Y. Xie, C. Xu and F. Zhang, *Nat. Commun.*, 2018, **9**, 2898.
84 S. Wang, L. Liu, Y. Fan, A. M. El-Toni, M. S. Alhoshan, D. Li and F. Zhang, *Nano Lett.*, 2019, **19**, 2418–2427.
85 S. Ling, X. Yang, C. Li, Y. Zhang, H. Yang, G. Chen and Q. Wang, *Angew. Chem., Int. Ed.*, 2020, **59**, 7219–7223.
86 Y. Xu, B. Li, P. Han, S. Sun and Y. Pang, *The Analyst*, 2013, **138**, 1004–1007.

87 L. Feng, C. Dou, Y. Xia, B. Li, M. Zhao, A. M. El-Toni, N. F. Atta, Y. Zheng, X. Cai, Y. Wang, Y. Cheng and F. Zhang, *Adv. Funct. Mater.*, 2020, **30**, 2006581.
88 B. Li, J. Lin, P. Huang and X. Chen, *Nanotheranostics*, 2022, **6**, 91–102.
89 N. Zhao, L. Yan, X. Zhao, X. Chen, A. Li, D. Zheng, X. Zhou, X. Dai and F. J. Xu, *Chem. Rev.*, 2019, **119**, 1666–1762.
90 B. Wang, X. He, Z. Zhang, Y. Zhao and W. Feng, *Acc. Mater. Res.*, 2013, **46**, 761–769.
91 H. Park, J. Kim, S. Jung and W. J. Kim, *Adv. Funct. Mater.*, 2018, **28**, 1705416.
92 X. Ge, Q. Fu, L. Su, Z. Li, W. Zhang, T. Chen, H. Yang and J. Song, *Theranostics*, 2020, **10**, 4809–4821.
93 B. Li, W. Li, Y. Xu, J. Li, J. Tu and S. Sun, *Chem. Commun.*, 2015, **51**, 14652–14655.
94 C. Sun, B. Li, M. Zhao, S. Wang, Z. Lei, L. Lu, H. Zhang, L. Feng, C. Dou, D. Yin, H. Xu, Y. Cheng and F. Zhang, *J. Am. Chem. Soc.*, 2019, **141**, 19221–19225.
95 L. Liu, S. Wang, B. Zhao, P. Pei, Y. Fan, X. Li and F. Zhang, *Angew. Chem., Int. Ed.*, 2018, **57**, 7518–7522.
96 X. Fu, J. Wu, H. Xu, P. Wan, H. Fu and Q. Mei, *Anal. Chem.*, 2021, **93**, 15696–15702.
97 C. Sun, M. Zhao, X. Zhu, P. Pei and F. Zhang, *CCS Chem.*, 2022, **4**, 476–486.
98 X. Wang, R. R. Valiev, T. Y. Ohulchanskyy, H. Agren, C. Yang and G. Chen, *Chem. Soc. Rev.*, 2017, **46**, 4150–4167.
99 Z. Liu, B. Yun, Y. Han, Z. Jiang, H. Zhu, F. Ren and Z. Li, *Adv. Healthcare Mater.*, 2022, **11**, e2102042.
100 G. Chen, J. Damasco, H. Qiu, W. Shao, T. Y. Ohulchanskyy, R. R. Valiev, X. Wu, G. Han, Y. Wang, C. Yang, H. Ågren and P. N. Prasad, *Nano Lett.*, 2015, **15**, 7400–7407.
101 Q. Liu, Y. Zhong, Y. Su, L. Zhao and J. Peng, *Nano Lett.*, 2021, **21**, 4606–4614.
102 C. Cao, X. Zhou, M. Xue, C. Han, W. Feng and F. Li, *ACS Appl. Mater. Interfaces*, 2019, **11**, 15298–15305.
103 T. Chen, Y. Zhang, R. Ao, L. Su, Y. Jiang, Y. Zhang, H. Cai, J. Wang, Q. Chen, J. Song, L. Lin, H. Yang, P. Hou and X. Chen, *Angew. Chem., Int. Ed.*, 2021, **60**, 15006–15012.
104 X. Ge, Y. Lou, L. Su, B. Chen, Z. Guo, S. Gao, W. Zhang, T. Chen, J. Song and H. Yang, *Anal. Chem.*, 2020, **92**, 6111–6120.
105 Y. Lyu, D. Cui, J. Huang, W. Fan, Y. Miao and K. Pu, *Angew. Chem., Int. Ed.*, 2019, **58**, 4983–4987.
106 W. Zeng, L. Wu, Y. Ishigaki, T. Harimoto, Y. Hu, Y. Sun, Y. Wang, T. Suzuki, H. Y. Chen and D. Ye, *Angew. Chem., Int. Ed.*, 2022, **61**, e202111759.
107 L. Lu, B. Li, S. Ding, Y. Fan, S. Wang, C. Sun, M. Zhao, C. X. Zhao and F. Zhang, *Nat. Commun.*, 2020, **11**, 4192.
108 W. Becker, *J. Microsc.*, 2012, **247**, 119–136.
109 D. H. Ortgies, M. Tan, E. C. Ximendes, B. del Rosal, J. Hu, L. Xu, X. Wang, E. Martin Rodriguez, C. Jacinto, N. Fernandez, G. Chen and D. Jaque, *ACS Nano*, 2018, **12**, 4362–4368.
110 Y. Cheng, R. M. Borum, A. E. Clark, Z. Jin, C. Moore, P. Fajtova, A. J. O'Donoghue, A. F. Carlin and J. V. Jokerst, *Angew. Chem., Int. Ed.*, 2022, **61**, e202113617.